Am J Physiol Heart Circ Physiol 291: H318–H326, 2006.
First published February 24, 2006; doi:10.1152/ajpheart.00975.2005.

Short-term electroacupuncture at Zusanli resets the arterial baroreflex neural arc toward lower sympathetic nerve activity

Daisaku Michikami,[1,2] Atsunori Kamiya,[1] Toru Kawada,[1] Masashi Inagaki,[1] Toshiaki Shishido,[1] Kenta Yamamoto,[1,2] Hideto Ariumi,[1,2] Satoshi Iwase,[3] Junichi Sugenoya,[3] Kenji Sunagawa,[4] and Masaru Sugimachi[1]

[1]*Department of Cardiovascular Dynamics, Advanced Medical Engineering Center, National Cardiovascular Center Research Institute, Osaka;* [2]*Pharmaceuticals and Medical Devices Agency, Tokyo;* [3]*Department of Physiology, School of Medicine Aichi Medical University, Nagakute, Aichi; and* [4]*Department of Cardiovascular Medicine, Kyushu University Graduate School of Medical Sciences, Fukuoka, Japan*

Submitted 12 September 2005; accepted in final form 17 February 2006

Michikami, Daisaku, Atsunori Kamiya, Toru Kawada, Masashi Inagaki, Toshiaki Shishido, Kenta Yamamoto, Hideto Ariumi, Satoshi Iwase, Junichi Sugenoya, Kenji Sunagawa, and Masaru Sugimachi. Short-term electroacupuncture at Zusanli resets the arterial baroreflex neural arc toward lower sympathetic nerve activity. *Am J Physiol Heart Circ Physiol* 291: H318–H326, 2006. First published February 24, 2006; doi:10.1152/ajpheart.00975.2005.—Although electroacupuncture reduces sympathetic nerve activity (SNA) and arterial pressure (AP), the effects of electroacupuncture on the arterial baroreflex remain to be systematically analyzed. We investigated the effects of electroacupuncture of Zusanli on the arterial baroreflex using an equilibrium diagram comprised of neural and peripheral arcs. In anesthetized, vagotomized, and aortic-denervated rabbits, we isolated carotid sinuses and changed intra-carotid sinus pressure (CSP) from 40 to 160 mmHg in increments of 20 mmHg/min while recording cardiac SNA and AP. Electroacupuncture of Zusanli was applied with a pulse duration of 5 ms and a frequency of 1 Hz. An electric current 10 times the minimal threshold current required for visible muscle twitches was used and was determined to be 4.8 ± 0.3 mA. Electroacupuncture for 8 min decreased SNA and AP (n = 6). It shifted the neural arc (i.e., CSP-SNA relationship) to lower SNA but did not affect the peripheral arc (i.e., SNA-AP relationship) (n = 8). SNA and AP at the closed-loop operating point, determined by the intersection of the neural and peripheral arcs, decreased from 100 ± 4 to 80 ± 9 arbitrary units and from 108 ± 9 to 99 ± 8 mmHg (each $P < 0.005$), respectively. Peroneal denervation eliminated the shift of neural arc by electroacupuncture (n = 6). Decreasing the pulse duration to <2.5 ms eliminated the effects of SNA and AP reduction. In conclusion, short-term electroacupuncture resets the neural arc to lower SNA, which moves the operating point toward lower AP and SNA under baroreflex closed-loop conditions.

arterial pressure; equilibrium diagram

ALTHOUGH THERE ARE MANY clinical case reports (21, 30, 32, 39, 40, 42), the effects of electroacupuncture on cardiovascular regulation remain to be systematically investigated. There has been a recent renewal of interest in the inhibitory effects of electroacupuncture of the Zusanli acupoint on the cardiovascular system, including reductions in arterial pressure (AP), heart rate, (3, 15, 16), and sympathetic nerve activity (SNA) (25, 42). Such inhibitory effects are observed during low-frequency (<20 Hz) electroacupuncture. Because the arterial baroreflex is one of the most important control systems that stabilize AP, we quantified the effects of electroacupuncture on the arterial baroreflex over an entire operating range. Systematic analysis would help to assess the possible utility of electroacupuncture as a treatment modality for certain cardiovascular diseases with vagolytic and sympathotonic states (26, 38).

One of the best ways to quantitatively analyze changes in the arterial baroreflex over an entire operating range may be analysis using a baroreflex equilibrium diagram (10, 23, 31) (see APPENDIX for details). Briefly, the baroreflex equilibrium diagram consists of a neural arc representing SNA as a function of baroreceptor input pressure and a peripheral arc representing AP as a function of SNA. The intersection of the two arcs corresponds to an operating point of the AP regulation under baroreflex closed-loop conditions. Considering the reduced AP and SNA found in previous studies, we hypothesized that short-term electroacupuncture resets the arterial baroreflex neural arc to lower SNA. In the present study, to test this hypothesis, we constructed a baroreflex equilibrium diagram with neural and peripheral arcs in anesthetized rabbits. The present findings indicate that electroacupuncture resets the baroreflex neural arc to lower SNA, moving the closed-loop operating point toward lower AP and SNA.

MATERIALS AND METHODS

Surgical Preparation

Animals were cared for in strict accordance with the *Guiding Principles for the Care and Use of Animals in the Field of Physiological Sciences* approved by the Physiological Society of Japan. Twenty-two Japanese White rabbits weighing 2.4–3.3 kg were anesthetized via intravenous injection (2 ml/kg) with a mixture of urethane (250 mg/ml) and α-chloralose (40 mg/ml) and mechanically ventilated with oxygen-enriched room air. Supplemental doses were injected as necessary (0.5 ml/kg) to maintain an appropriate level of anesthesia. Body temperature was maintained at ~38°C with a heating pad. AP was measured by using a high-fidelity pressure transducer (SPC-330A, Millar Instruments, Houston, TX) inserted via the left femoral artery. To record cardiac SNA, we exposed the left cardiac sympathetic nerve through a midline thoracotomy and attached a pair of stainless steel wire electrodes (Bioflex wire AS633, Cooner Wire, Chatsworth, CA) to the nerve. The nerve fibers peripheral to the

Address for reprint requests and other correspondence: D. Michikami, Dept. of Cardiovascular Dynamics, Advanced Medical Engineering Center, National Cardiovascular Center Research Institute, 5–7-1 Fujishirodai, Suita, Osaka 565–8565, Japan (e-mail: dmichi@ri.ncvc.go.jp or kamiya@ri.ncyc.go.jp).

The costs of publication of this article were defrayed in part by the payment of page charges. The article must therefore be hereby marked "*advertisement*" in accordance with 18 U.S.C. Section 1734 solely to indicate this fact.

0363-6135/06 $8.00 Copyright © 2006 the American Physiological Society

electrodes were sectioned to eliminate afferent signals from the heart. To insulate and fix the electrodes, the nerves and electrodes were secured with silicone glue (Kwik-Sil, World Precision Instruments, Sarasota, FL). The preamplified nerve signals were band-pass filtered at 150–1,000 Hz, full-wave rectified, and low-pass filtered at a cutoff frequency of 30 Hz by using analog circuit. After that, the neural signals were recorded at a sampling rate of 200 Hz using a 12-bit analog-to-digital converter. Pancuronium bromide (0.1 mg/kg) was administered to prevent contaminating muscular activities. At the end of the experiment, the experimental animals were killed by an overdose of intravenous pentobarbital sodium, and the background noise level of SNA was determined postmortem.

Sixteen of the 22 rabbits were used in *protocol 1 (protocols 1-1, 1-2, and 1-3)*, and the remaining 6 rabbits were used in *protocols 2, 3,* and *4*. In 10 of the 16 rabbits for *protocols 1-2* and/or *1-3* described below, we isolated both carotid sinuses from the systemic circulation by ligating the internal and external carotid arteries and other small branches originating from the carotid sinus regions. The isolated carotid sinuses were filled with warmed physiological saline through catheters inserted via the common carotid arteries. The intra-carotid sinus pressure (CSP) was controlled by a servo-controlled piston pump (model ET-126A, Labworks, Costa Mesa, CA). In the baroreflex open-loop experimental settings, bilateral vagal and aortic depressor nerves were sectioned at the neck to minimize reflex effects from cardiopulmonary regions and the aortic arch.

Electroacupuncture

Two stainless steel needles were inserted at the one-fifth point (from the knee) and the midpoint of the knee-ankle distance of approximately 30–35 mm. These needles with a diameter of 0.2 mm (CE0123, Seirin-Kasei, Shimizu City, Japan) were inserted to a depth of ~10 mm in the skin and underlying muscle (the right tibialis anterior muscle). This area corresponds to the Zusanli and Xiajuxu acupoints (over the peroneal nerve below the knee, stomach meridian, St 36 and 39) in humans.

As in previous studies (2, 3, 17, 42), the stimulus current intensity was determined as 10 times of twitch threshold, which is the minimal electrical current required for eliciting visible muscle twitches of the stimulated leg. Actually, the current was 4.8 ± 0.3 mA (4.2–5.4 mA). An electric rectangular wave current with a frequency of 1 Hz and with pulse duration of 5 ms was passed between these two needles by using an electrical stimulator (SEN-7203, Nihon Kohden) except *protocol 4* where shorter pulse durations were challenged.

Protocols

The experimental protocol was approved by the Animal Experimental Committee of National Cardiovascular Center Research Institute.

Protocol 1: effect of Zusanli electroacupuncture on AP, SNA, and baroreflex. PROTOCOL 1-1 (BAROREFLEX CLOSED-LOOP CONDITION, N = 6). To elucidate the overall cardiovascular inhibitory effects of electroacupuncture, we performed 1 Hz electroacupuncture for 8 min and measured AP and SNA responses under conditions of intact cardiovascular reflexes. In this closed-loop protocol, vagal and aortic depressor nerves were preserved. Baseline data were measured for 1 min before acupuncture insertion. At 10 min after acupuncture insertion, baseline data were measured again for 1 min. Electroacupuncture was applied for 8 min. The recovery data were measured for 2 min after the cessation of electroacupuncture.

PROTOCOL 1-2 (BAROREFLEX OPEN-LOOP CONDITION, N = 8). To elucidate the effects of electroacupuncture on the arterial baroreflex over an entire operating range, we performed a baroreflex open-loop experiment as follows. CSP was first decreased to 40 mmHg. After attainment of a steady state, CSP was increased from 40 to 160 mmHg in increments of 20 mmHg. Each pressure step was maintained for 60 s. We measured AP and SNA during the stepwise increase in CSP. Two trials (control and electroacupuncture trials) were performed on each rabbit. The order of the trials was randomized. The electroacupuncture trial was identical to the control trial except that electroacupuncture was commenced 1 min before the initiation of stepwise increase in CSP.

PROTOCOL 1-3 (BAROREFLEX OPEN-LOOP CONDITION WITH PERONEAL DENERVATION, N = 6). To identify the afferent pathway of electroacupuncture, we examined the effects of 1 Hz electroacupuncture on the arterial baroreflex after severing the right peroneal nerve at the level of the knee joint. Estimation of the baroreflex equilibrium diagram was conducted as in *protocol 1-2* in the control and electroacupuncture trials. Four of the six rabbits had also undergone *protocol 1-2*.

Protocol 2: effects of sham (nonelectrical) acupuncture at Zusanli and control (nonspecific) electrical and nonelectrical acupunctures on AP and SNA in baroreflex closed-loop condition (n = 6). To determine whether changes in AP and SNA during Zusanli electroacupuncture are specific responses, sham and control acupunctures were conducted under the following acupuncture conditions: *1*) no acupuncture (nonacupuncture), *2*) nonelectrical acupuncture at Zusanli-Xiajuxu (St 36–39) acupoints (sham acupuncture), *3*) nonelectrical acupuncture at Guangming-Xuanzhong (gallbladder meridian, Gb 37–39) acupoints (control acupuncture), and *4*) electrical acupuncture at Guangming-Xuanzhong acupoints (control electroacupuncture). We chose Guangming-Xuanzhong as nonspecific control acupoints (*trials 3* and *4*) because these acupoints are believed to reduce leg pain without affecting the cardiovascular system, in contrast to the Zusanli-Xiajuxu acupoints. In each trial, AP and SNA were measured for a baseline duration of 1 min, under acupuncture condition (*trial 1, 2, 3,* or *4*) for 8 min, and recovery for 1 min.

Protocol 3: effect of long-term Zusanli electroacupuncture on AP and SNA in baroreflex closed-loop condition (n = 6). To clarify the effect of long-term electroacupuncture on cardiovascular system, AP and SNA were measured during and after 30 min of electroacupuncture at Zusanli-Xiajuxu acupoints. *Protocol 3* was conducted in the same manner as *protocol 1-1* except with a longer stimulation duration than *protocol 1-1* (8 min).

Protocol 4: Effect of pulse duration of Zusanli electroacupuncture on AP and SNA in baroreflex closed-loop condition (n = 6). To examine the effect of pulse duration of electroacupuncture on AP and SNA, AP and SNA were measured during electroacupuncture at Zusanli-Xiajuxu acupoints with the pulse duration increasing stepwise from 0.1 to 0.25, 0.5, 1, 2.5, 5, and 10 ms, every 60 s. In each animal, the frequency and stimulus current intensity were maintained constant as in *protocols 1, 2,* and *3*.

Data Analysis

We recorded CSP, SNA, and AP at a sampling rate of 200 Hz by using a 12-bit analog-to-digital converter. Data were stored on the hard drive of a dedicated laboratory computer system for later analyses.

In *protocol 1-1, 2, and 4*, mean AP and SNA for 1 min were calculated for baseline conditions, every minute of electroacupuncture, and recovery. In *protocol 3*, mean AP and SNA for 5 min were calculated for baseline conditions, electroacupuncture, and recovery. In *protocols 1-2* and *1-3*, we calculated mean AP and SNA during the last 10 s of each CSP step. Because the absolute magnitude of SNA depended on recording conditions, SNA was presented in arbitrary units (au). The background noise level was set at 0 au and the SNA value at the closed-loop operating point in the control trial (without electroacupuncture) was set at 100 au for each animal.

A four-parameter logistic function analysis was performed on the neural arc (CSP-SNA data pairs) and the peripheral arc (SNA-AP data pairs) as follows (11)

$$y = \frac{P_1}{1 + \exp[P_2(x - P_3)]} + P_4 \quad (1)$$

where x and y represent the input and the output, respectively. P_1 denotes the response range (i.e., the difference between the maximum and minimum values of y), P_2 is the coefficient of gain, P_3 is the midpoint of the logistic function on the input axis, and P_4 is the minimum value of y. The maximum gain (G_{max}) is calculated from $-P_1P_2/4$ at $x = P_3$. The parameter values were calculated by an iterative nonlinear least-squares regression known as the downhill simplex method.

Statistical Analysis

All data are presented as means ± SD. Differences were considered to be significant when $P < 0.05$. In *protocols 1-1, 2, 3,* and *4*, the effects of electroacupuncture on AP and SNA at different time intervals were evaluated by one-way ANOVA. The Dunnett's test was used for multiple comparisons. In *protocols 1-2* and *1-3*, the effects of electroacupuncture on the four parameters of the logistic functions relating to the neural and peripheral arcs, as well as on the closed-loop operating point, were examined by using a paired *t*-test.

RESULTS

Figure 1*A* (*protocol 1-1*) shows a typical time series of AP and SNA in response to Zusanli-Xiajuxu electroacupuncture with intact cardiovascular reflexes. AP and SNA were reduced immediately after beginning electroacupuncture, and these remained reduced during 8-min electroacupuncture. Figure 1*B* illustrates the group-averaged AP and SNA in response to electroacupuncture. AP and SNA for baseline were unchanged by acupuncture insertion alone, while these values for 8-min electroacupuncture remained decreased from baseline. These values returned to baseline level after the cessation of electroacupuncture.

Figure 2 (*protocol 1-2*) shows a typical AP and SNA response to the increments in CSP in the control (Fig. 2, *left*) and electroacupuncture (Fig. 2, *right*) trials. A stepwise increase in CSP decreased SNA and AP in both trials. In the electroacupuncture trial, the AP and SNA response ranges to CSP were attenuated compared with the control trial.

Figure 3, *A* and *B* (*protocol 1-2*), shows the averaged baroreflex neural and peripheral arcs obtained in control and electroacupuncture trials. The neural arc showed a sigmoidal relationship between CSP and SNA. In the neural arc, the response range of SNA (P_1) and midpoint of the operating range (P_3) were significantly decreased by electroacupuncture (Table 1). The coefficient of gain (P_2), the minimum value of SNA (P_4), and G_{max} did not differ between the two trials (Table 1). As a result, the maximum value of SNA, calculated from $P_1 + P_4$, was significantly decreased by electroacupuncture from 162 ± 31 to 130 ± 29 au ($P < 0.005$). The peripheral arc showed a more linear relationship between SNA and AP than the neural arc. In the peripheral arc, electroacupuncture did not affect any of the four parameters or G_{max} (Table 1 and Fig. 3*B*). The operating point determined by the intersection of the neural and peripheral arcs was moved toward lower AP and SNA (from *point a* to *point b*) by electroacupuncture (Fig. 3*C* and Table 1).

Figure 4 (*protocol 1-3*) shows the averaged baroreflex neural (Fig. 4*A*) and peripheral arcs (Fig. 4*B*) in control and electroacupuncture trials with severance of the peroneal nerve innervating the tibialis anterior muscle. Two arcs obtained in both trials were nearly superimposable. The four parameters and G_{max} in the neural and peripheral arcs and operating point were

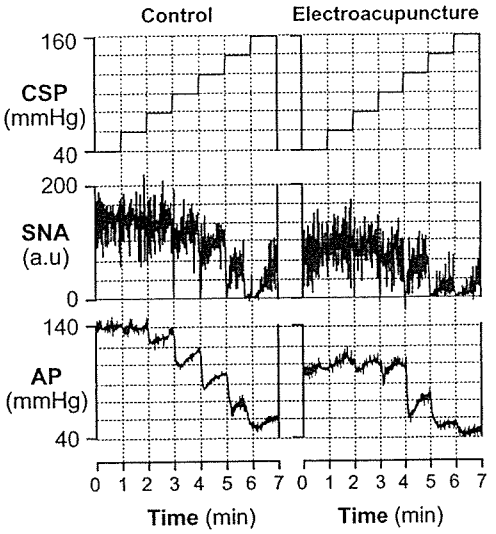

Fig. 2. Typical time series of intra-carotid sinus pressure (CSP), AP, and SNA in control (*left*) and electroacupuncture trials (*right*) in *protocol 1-2*. SNA and AP decreased in response to increments in CSP in both of the two trials. The response ranges of AP and SNA to CSP were lower in electroacupuncture than in controls.

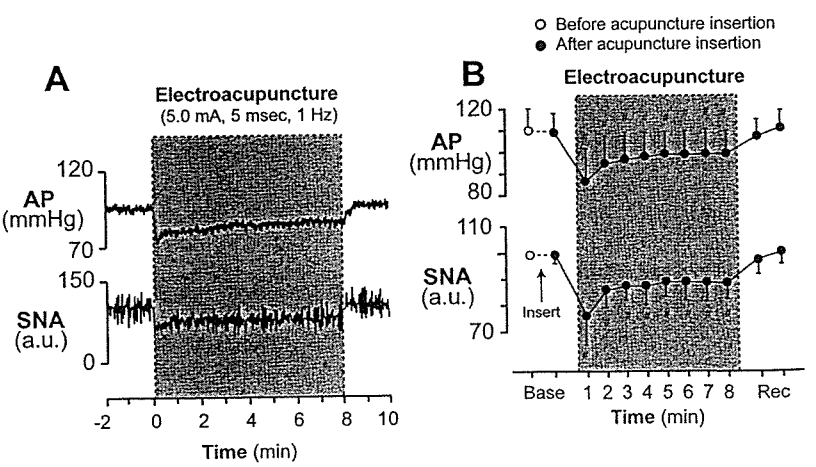

Fig. 1. Typical time series of arterial pressure (AP) and sympathetic nerve activity (SNA) during 8 min of 1-Hz electroacupuncture (*A*) and the averaged ($n = 6$) AP and SNA (*B*) in *protocol 1-1*. Data include periods of baseline (Base, 1 min), electroacupuncture (8 min), and recovery (Rec, 1 min). Each data point represents average values over 1 min. #$P < 0.05$: significantly different from baseline after acupuncture insertion. au, Arbitrary units.

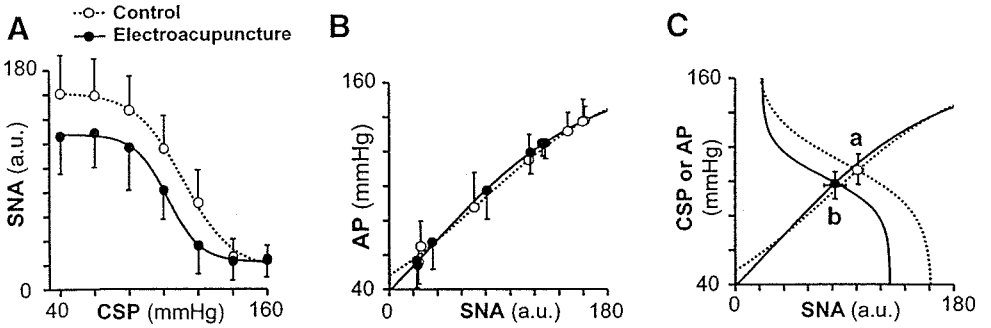

Fig. 3. Averaged (n = 8) baroreflex neural arc (A), peripheral arc (B), and baroreflex equilibrium diagram (C) obtained in 8 rabbits in control (○) and electroacupuncture (●) trials in *protocol 1-2*. Electroacupuncture shifted the neural arc to lower SNA (A), but it did not change the peripheral arc (B). The shift in neural arc reduced AP and SNA by 9 ± 3 mmHg and 20 ± 10 au (from *point a* to *point b*) at the operating point (C).

not affected by electroacupuncture when the peroneal nerve was denervated (Table 2 and Fig. 4*C*).

Figure 5 (*protocol 2*) shows the changes in AP and SNA during nonacupuncture (without acupuncture), sham acupuncture [nonelectrical acupuncture at Zusanli-Xiajuxu (St 36–39)], control acupuncture [nonelectrical acupuncture at Guangming-Xuanzhong (Gb 37–39)] and control electroacupuncture (electrical acupuncture at Gb 37–39) trials. AP and SNA did not change in these trials.

Figure 6, *A* and *B* (*protocol 3*), shows a typical time series and the averaged data, respectively, of AP and SNA in response to long-term Zusanli-Xiajuxu electroacupuncture. AP and SNA decreased immediately after electroacupuncture was started and remained reduced during 30-min electroacupuncture. In addition, AP and SNA returned to the preelectroacupuncture baseline levels immediately after cessation of electroacupuncture.

Figure 7, *A* and *B* (*protocol 4*), shows a typical time series and the averaged data, respectively, of AP and SNA during Zusanli-Xiajuxu electroacupuncture with the pulse duration increasing from 0.1 to 5 ms. Although increasing the pulse duration from 0.1 to 1 ms did not change AP and SNA, pulse durations of 2.5 ms and higher decreased SNA while pulse durations of 5 and 10 ms decreased AP.

Table 1. *Effect of electroacupuncture on the operating point of baroreflex and on the 4 parameters of logistic functions approximating neural and peripheral baroreflex arcs*

	Control	Electroacupuncture
Operating point		
Arterial pressure, mmHg	108.4±8.7	98.8±7.9†
Sympathetic nerve activity, au	99.8±4.1	80.0±8.9†
Neural arc		
P_1, au	144.0±35.0	112.6±9.2†
P_2, au/mmHg	0.08±0.03	0.09±0.09
P_3, mmHg	111.4±6.5	103.3±10.0*
P_4, au	17.5±6.1	17.4±8.7
G_{max}, au/mmHg	−2.94±0.91	−2.58±1.27
Peripheral arc		
P_1, mmHg	129.6±20.5	125.9±19.5
P_2, au/mmHg	−0.03±0.01	−0.03±0.01
P_3, au	80.6±23.2	71.7±17.1
P_4, mmHg	29.9±16.3	29.5±12.1
G_{max}, mmHg/au	0.74±0.10	0.84±0.18

Values are means ± SD (n = 8). G_{max}, maximum gain. See *Data Analysis* for definition of 4 parameters of logistic function. au, Arbitrary units. *P < 0.05 and †P < 0.005 vs. control.

DISCUSSION

The major new finding of the present study was that electroacupuncture at Zusanli resets the arterial baroreflex neural arc to lower SNA but does not significantly affect the baroreflex peripheral arc. As a result, the operating point determined by the intersection of the neural and peripheral arcs was moved toward lower SNA and AP by electroacupuncture. To the best of our knowledge, this is the first study delineating the effects of short-term electroacupuncture on the arterial baroreflex over an entire operating range.

Effects of Electroacupuncture on the Arterial Baroreflex (Protocol 1)

The arterial baroreflex system is one of the most important negative-feedback systems that stabilize AP against exogenous disturbances. When AP is decreased by exogenous perturbation such as blood loss, the reduction in AP is sensed by the arterial baroreceptors. SNA is then increased by the arterial baroreflex to buffer the reduction in AP. In such circumstances, SNA and AP change reciprocally. On the other hand, when SNA is changed by an exogenous perturbation such as emotional stress, SNA and AP change in parallel. In *protocol 1-1*, electroacupuncture decreased both SNA and AP, indicating that electroacupuncture introduced exogenous perturbation to decrease SNA with a resultant reduction in AP. Although the net effect of electroacupuncture is to decrease SNA, the perturbation of AP cannot be excluded. For example, because electroacupuncture also twitched the hindlimb muscles, electroacupuncture might have perturbed AP via changes in vascular resistance and/or venous return through muscle pump function. Therefore, to quantify the contribution of both perturbations on SNA and on AP, we performed *protocol 1-2*. Perturbation of AP is most easily detected by comparing AP at the same SNA level with and without electroacupuncture.

In *protocol 1-2*, we performed a baroreflex open-loop experiment and identified the static characteristics of the neural and peripheral arcs over a wide operating range. As expected, electroacupuncture shifted the neural arc toward lower SNA and decreased maximum SNA to ~80% of control (Fig. 3*A*). This shift is not due to reduced perfusion to the medulla by AP reduction during electroacupuncture because the AP was decreased by ~10 mmHg and would not induce cerebral ischemia. In contrast, electroacupuncture had little effect on the peripheral arc (Fig. 3*B*). In other words, AP with and without electroacupuncture did not differ significantly at any of the SNA levels. Therefore, changes in AP observed in *protocol 1-1*

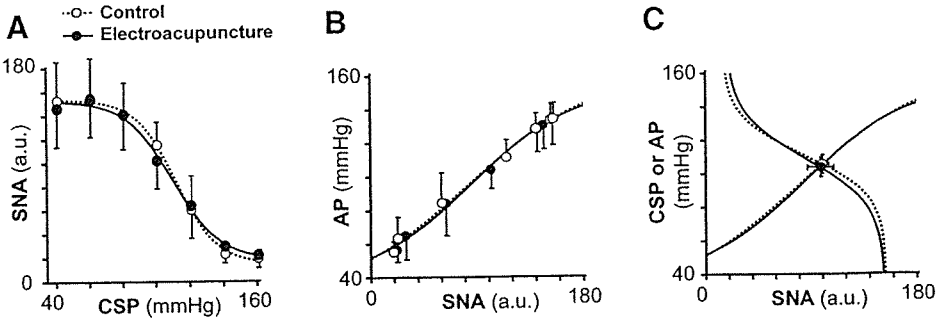

Fig. 4. Averaged (n = 6) baroreflex neural arc (A), peripheral arc (B), and baroreflex equilibrium diagrams (C) obtained in 6 rabbits in control (○) and electroacupuncture (●) trials with peroneal denervation in *protocol 1-3*. The baroreflex neural arc, peripheral arc, and the operating point were not influenced by electroacupuncture after peroneal denervation.

were attributable exclusively to perturbation of SNA and not to possible perturbation effects of electroacupuncture on AP.

The neural and peripheral arcs were combined to yield a baroreflex equilibrium diagram (Fig. 3*C*). The closed-loop operating point, determined by the intersection of the neural and peripheral arcs, moved from *point a* to *point b* during electroacupuncture. Despite a significant shift in the closed-loop operating point, neither the neural nor peripheral arc gain was altered significantly (Table 1). The fact that the baroreflex gain was maintained during electroacupuncture suggests the possible application of electroacupuncture to the treatment of cardiovascular diseases with sympathetic hyperactivity. However, the preservation of the arterial baroreflex gain in the present experimental settings may rely on normal peripheral arc characteristics. Cardiovascular diseases such as heart failure may decrease the peripheral arc gain to a variable extent due to impaired pump function. Whether the arterial baroreflex function during electroacupuncture can be maintained in cardiovascular diseases awaits future study.

Mechanisms for the Cardiovascular Inhibitory Effects of Electroacupuncture (Protocol 1)

The resetting in the baroreflex neural arc during electroacupuncture was mediated by a somatosympathetic reflex arising from the stimulated hindlimb, as evidenced by the fact that peroneal denervation abolished the resetting (Table 2 and Fig. 4). This result was consistent with an earlier study (27) showing that depressor and sympathoinhibitory responses during acupuncture were abolished by sciatic and femoral denervation. The existence of a somatosympathetic reflex is also supported by the fact that electrical stimulation of somatic afferents reduced AP (7–9). Legramante et al. (14) showed that rapidly conducting group III somatic afferent activation can evoke AP reduction during 1-Hz electrical stimulation of the tibial nerve. In contrast, high-frequency stimulation of the somatic afferent evokes AP elevation. Passive muscle stretching, which is considered to activate group III somatic afferent fibers, shifts the baroreflex neural arc toward higher SNA, resulting in an increase in the closed-loop operating point (41). The mechanism of two opposing influences of somatic afferent activation depending on the stimulation frequency is not fully understood.

Table 2. *Effect of electroacupuncture with peroneal denervation on the operating point of baroreflex and on the 4 parameters of logistic functions approximating neural and peripheral baroreflex arcs*

	Control	Electroacupuncture
Operating point		
Arterial pressure, mmHg	105.7±5.7	104.1±5.6
Sympathetic nerve activity, au	99.8±5.1	98.3±11.1
Neural arc		
P_1, au	138.3±42.4	136.3±38.6
P_2, au/mmHg	0.11±0.03	0.08±0.03
P_3, mmHg	112.7±10.2	111.5±10.6
P_4, au	14.9±8.7	15.7±7.4
G_{max}, au/mmHg	−3.27±1.15	−2.84±1.12
Peripheral arc		
P_1, mmHg	144.1±35.5	140.5±34.4
P_2, au/mmHg	−0.02±0.002	−0.02±0.004
P_3, au	82.0±34.0	78.8±32.0
P_4, mmHg	26.1±8.1	25.5±5.3
G_{max}, mmHg/au	0.69±0.13	0.72±0.21

Values are means ± SD (n = 6). See *Data Analysis* for definition of 4 parameters of logistic function.

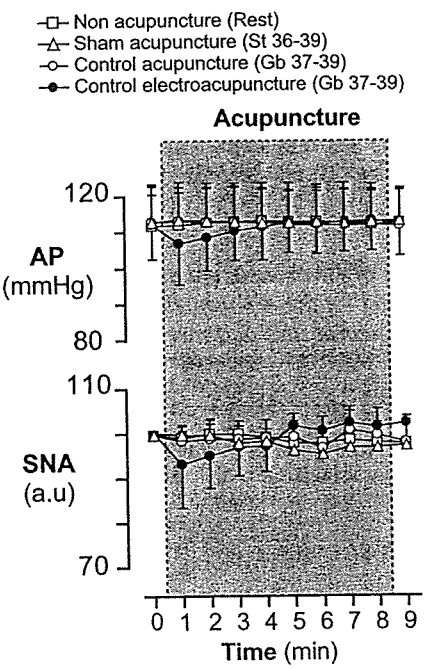

Fig. 5. Averaged (n = 6) AP (*top*) and SNA (*bottom*) in nonacupuncture (condition without acupuncture, □), sham acupuncture [nonelectrical acupuncture at Zusanli-Xiajuxu (stomach meridian, St 36–39), △], control acupuncture [nonelectrical and acupuncture at Guangming-Xuanzhong (gallbladder meridien, Gb 37–39), ○], and control electroacupuncture [electrical acupuncture at Gb 37–39, ●] trials in *protocol 2*. Data include periods of baseline (1 min), electroacupuncture (8 min), and recovery (1 min). Each data point represents average values over 1 min.

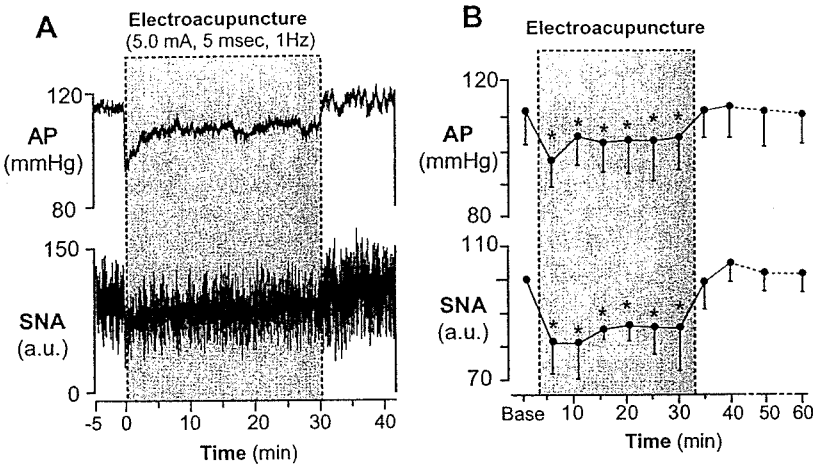

Fig. 6. Typical time series of AP and SNA during 30 min of 1-Hz electroacupuncture (St 36–39; *A*) and the averaged (n = 6) AP and SNA (*B*) in *protocol 3*. Data include periods of baseline (5 min), electroacupuncture (30 min), and recovery (30 min). Each data point represents averaged values over 5 min during baseline, electroacupuncture, and the first 10 min of recovery and those over 10 min during the last 20 min of recovery. *$P < 0.05$: significantly different from baseline after acupuncture insertion.

Another explanation for resetting in the neural arc may be circulatory endogenous opioids (e.g., β-endorphin and enkephalin), which are released from the adrenal gland and hypothalamus by prolonged (>30 min) electroacupuncture (20, 21). These endogenous opioids are known to modulate the arterial baroreflex (24, 29, 35). However, changes in endogenous opioids are unlikely to be the mechanism for reductions in SNA and AP by electroacupuncture in the present experimental settings because the inhibitory effects terminated immediately after cessation of electroacupuncture rather than lasting for several hours (42) (Fig. 1).

Previous studies suggest a central interaction between an electroacupuncture-evoked somatosympathetic reflex and the arterial baroreflex. Baroreceptor afferent inputs inhibit neural activities in the rostral ventrolateral medulla (rVLM) (6, 33). Tjen-A-Looi et al. (36) showed that electroacupuncture inhibited rVLM neural activities, suggesting that the electroacupuncture-evoked somatosympathetic reflex and arterial baroreflex share common central pathways. In addition, 2-Hz electroacupuncture inhibits SNA through the excitation of β-endorphinergic and GABAergic neurons to rVLM (12, 13).

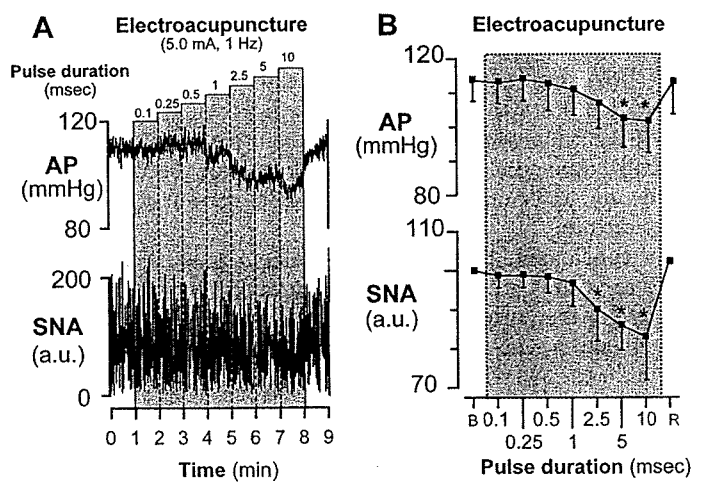

Fig. 7. Typical time series of AP and SNA during 1-Hz electroacupuncture with increasing the pulse duration (*A*) and the averaged (n = 6) AP and SNA (*B*) in *protocol 4*. Data include periods of baseline (B, 1 min), electroacupuncture (7 min), and recovery (R, 1 min). Each data point represents average values over 1 min. *$P < 0.05$; significantly different from baseline after acupuncture insertion.

Central interaction in the brain stem may be involved in the resetting of the arterial baroreflex neural arc induced by electroacupuncture.

Characteristics of Zusanli-Xiajuxu Electroacupuncture Used in the Present Study

The Zusanli electroacupuncture used in this study has some unique characteristics. First, our results showed that baseline AP and SNA were decreased significantly by electroacupuncture, in contrast to previous studies that found no significant reduction in baseline AP and SNA during Zusanli electroacupuncture in rats (0.5-ms duration, 1–2 mA, 2 Hz) (18) and nonelectrical acupuncture in normotensive humans (right large intestine 4, right liver 3, and left spleen 6) (22). Second, our result showed that AP and SNA were reduced as soon as electroacupuncture was started, in contrast to previous reports that the effect of Zusanli electroacupuncture did not even begin to manifest for the first 10–15 min in rats (0.5-ms duration, 1–2 mA, 2 Hz) (18) and cats (0.5-ms duration, 0.4–0.6 mA, 2–4 Hz) (37). These discrepancies may be related to the differences in acupoints and stimulation conditions (pulse duration, current, and frequency). In particular, the pulse duration used in our study (5 ms) was approximately 10–50 times longer than that used in previous studies. Indeed, the data obtained from *protocol 4* show that increasing the pulse duration augments the reduction in AP and SNA during electroacupuncture; pulse durations shorter than 2.5 ms did not change AP and SNA, whereas durations of 2.5 ms and above decreased both parameters immediately after the electroacupuncture was started (Fig. 7). In addition, our data suggest that stimulation duration (<2.5 ms) does not affect arterial baroreflex, consistent with our preliminary data that baroreflex neural, peripheral, and total arcs remained unchanged during electroacupuncture with pulse durations <2.5 ms (unpublished data). These observations may indicate that the effect of electroacupuncture on arterial baroreflex is linked to the stimulation pulse duration.

The third characteristic is that the inhibitory effects of electroacupuncture on AP and SNA disappeared immediately after the cessation of electroacupuncture. In contrast, some studies showed that the inhibitory effects of electroacupuncture on AP lasted for 10–60 min after the cessation (18). The characteristics in this study may not be explained by the length of electroacupuncture because AP and SNA recovered to the

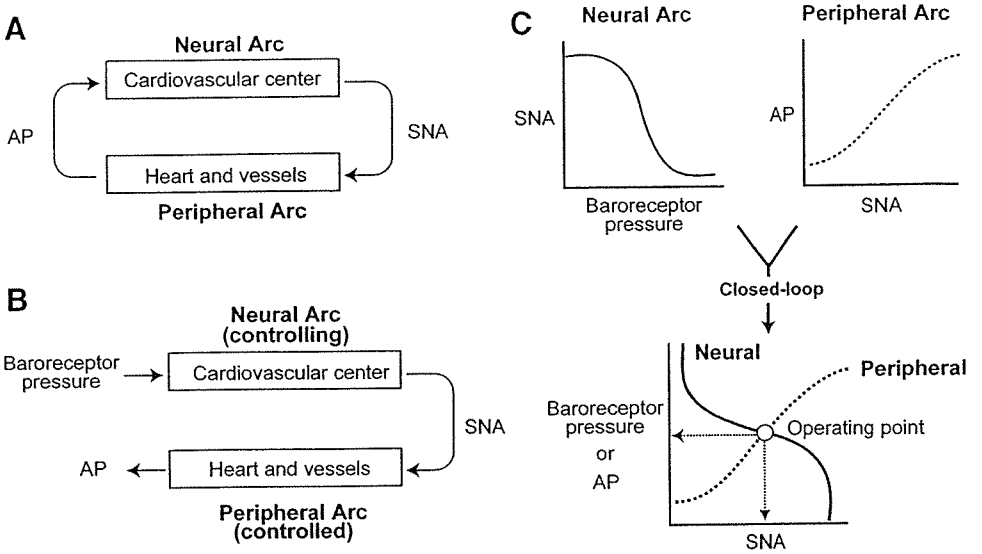

Fig. 8. Arterial baroreflex system in closed-loop (*A*) and open-loop (*B*) conditions. In open-loop conditions, the relationships between baroreceptor pressure and SNA (the neural arc) and between SNA and AP (the peripheral arc) can be quantitatively measured. Intersection of the neural and peripheral arcs corresponds to the operating point of AP and SNA under closed-loop conditions of feedback (*C*).

prestimulation baseline levels immediately after the cessation in both short-duration (8 min, Fig. 1) and longer-duration electroacupuncture (30 min, Fig. 6) protocols. The rapid disappearance of effects suggests that the AP and SNA reductions seen in the present study may not be elicited by the opioid mechanism, although clinical experiments with longer-duration electroacupuncture have demonstrated long-lasting effects on the cardiovascular system, which are attributed to opioid substances (2, 12, 15, 37, 42).

The reductions in AP and SNA during Zusanli electroacupuncture seen in the present study may not be just a nonspecific response to acupunctures. Our data from *protocol 2* (Fig. 5) showed that nonelectrical acupuncture at Zusanli (sham acupuncture) did not decrease AP and SNA, suggesting that the AP and SNA reductions during Zusanli electroacupuncture are not simply the results from insertion of acupuncture needles. Furthermore, acupuncture at Guangming-Xuanzhong (control acupuncture, control electroacupuncture) did not change AP and SNA regardless of electrical stimulation (Fig. 5). This result suggests the importance of acupoint specificity and is consistent with an earlier study showing point-specific differences in cardiovascular inhibitory responses (Jiangshi-Neiguan or Shousanli-Quchi acupoints vs. Pianli-Wenlui or Zusanli-Shangjuxu acupoints) (37). These observations may support the concept that Zusanli acupuncture changes cardiovascular variables in experimental animal models (4, 25, 28) and confers beneficial effects on cardiovascular diseases (5, 30, 34), whereas Guangming-Xuanzhong acupuncture does not affect cardiovascular variables (18).

Limitations

There are several limitations to this study. First, as anesthesia affects the autonomic nervous system, the results might have been different without anesthesia. Second, our isolation of the carotid sinus regions may stimulate carotid chemoreceptors. However, in determining baroreflex function, this factor was present in trials with and without electroacupuncture. Therefore, we believe that this factor may not affect our conclusion of baroreflex resetting during electroacupuncture.

Third, acupuncture was inserted at a point corresponding to the Zusanli acupoint in humans. When acupuncture is properly inserted at the acupoint, the patient feels heaviness or soreness. Such sensory information is not available in an anesthetized animal. Because electroacupuncture (as distinct from acupuncture with no electrical stimulation) stimulates not only the inserted point but also the surrounding area, it has been used as a convenient way of stimulating acupoints in patients and in experimental animals. Thus, even if we failed to insert the needle at the precise acupoint, we believe that Zusanli could be stimulated electrically.

Fourth, although we determined the effects of electroacupuncture at Zusanli acupoints on cardiovascular and baroreflex systems, there are other important acupoints that are able to influence these systems. In particular, Neiguan electroacupuncture is actually known to decrease sympathetic premotor neuron activity for a longer period than Zusanli electroacupuncture (36, 37). Further studies are necessary to determine the effect of Neiguan electroacupuncture on the arterial baroreflex.

Last, we evaluated the effects of Zusanli electroacupuncture on the baroreflex function for a short acupuncture duration of only 8 min. Because electroacupuncture is typically practiced for longer periods of time, our results have limited applicability. However, the electroacupuncture we used decreased AP and SNA immediately after application, showing that the procedure has acute effect on the cardiovascular system. That was the reason why we focused on the effect of short duration electroacupuncture on the baroreflex system. Future study is necessary to examine the effects of longer-duration electroacupuncture.

In conclusion, 1 Hz, short-term electroacupuncture of Zusanli reset the baroreflex neural arc toward lower SNA but did not affect the peripheral arc. The closed-loop operating point determined by the intersection of the neural and peripheral arcs was moved toward lower SNA and AP by electroacupuncture.

APPENDIX

Theoretical Considerations: Coupling of Neural and Peripheral Arcs

Changes in AP are immediately sensed by arterial baroreceptors, which alter efferent SNA via the cardiovascular center of baroreflex (Fig. 8*A*). Efferent SNA in turn governs heart rate and the mechanical

properties of the heart and vessels, which themselves exert a direct influence over AP. This negative-feedback loop makes it difficult to analyze the behavior of the arterial baroreflex. To overcome this problem, we opened the negative-feedback loop and divided the system into controlling and controlled elements (31). We defined the controlling element as the neural arc and the controlled element as the peripheral arc (Fig. 8*B*). In the neural arc, the input is the pressure sensed by the arterial baroreceptors and the output is SNA. In the peripheral arc, the input is SNA and the output is AP (Fig. 8*C*). Because pressure sensed by the arterial baroreceptor is equilibrated with AP under physiological conditions, we superimposed the functions of the two arcs and determined the operating point of the system from the intersection of the two arcs. The operating point is defined as the AP and SNA under closed-loop conditions of the feedback system. The validity of this framework has been examined in previous studies (10, 31). Using the baroreflex equilibrium diagram, we aimed to quantify the effects of electroacupuncture on the arterial baroreflex.

GRANTS

This study was supported by Health and Labor Sciences Research Grant for Research on Advanced Medical Technology from the Ministry of Health, Labour, and Welfare of Japan (H14-Nano-002), by a Grant-in-Aid for Scientific Research (A) (15200040) from the Japan Society for the Promotion of Science, the Program for Promotion of Fundamental Studies in Health Science from the Pharmaceutical and Medical Devices Agency of Japan, and by the "Ground-based Research Announcement for Space Utilization" project promoted by Japan Space Forum. This study was also supported by Industrial Technology Research Grant Program in 03A47075 from New Energy and Industrial Technology Development Organization (NEDO) of Japan.

REFERENCES

1. **Brickman AL, Calaresu FR, and Mogenson GJ.** Bradycardia during stimulation of the septum and somatic afferents in the rabbit. *Am J Physiol Regul Integr Comp Physiol* 236: R225–R230, 1979.
2. **Chao DM, Shen LL, Tjen-A-Looi S, Pitsillides KF, Li P, and Longhurst JC.** Naloxone reverses inhibitory effect of electroacupuncture on sympathetic cardiovascular reflex responses. *Am J Physiol Heart Circ Physiol* 276: H2127–H2134, 1999.
3. **Chen S and Ma SX.** Nitric oxide in the gracile nucleus mediates depressor response to acupuncture (ST36). *J Neurophysiol* 90: 780–785, 2003.
4. **Chiu DTJ and Cheng KK.** A study of the mechanism of the hypotensive effect of acupuncture in the rat. *Am J Chin Med* 2: 413–419, 1974.
5. **Chiu YJ, Chi A, and Reid IA.** Cardiovascular and endocrine effects of acupuncture in hypertensive patients. *Clin Exp Hypertens* 19: 1047–1063, 1997.
6. **Dampney RA, Horiuchi J, Tagawa T, Fontes MA, Potts PD, and Polson JW.** Medullary and supramedullary mechanisms regulating sympathetic vasomotor tone. *Acta Physiol Scand* 177: 209–218, 2003.
7. **Johansson B.** Studies on cardiovascular responses induced by electrical stimulation of afferent somatic nerves. A preliminary report. *Med Exp Int J Exp Med* 5: 447–453, 1961.
8. **Johansson B.** Circulatory responses to stimulation of somatic afferents with special reference to depressor effects from muscle nerves. *Acta Physiol Scand Suppl* 198: 1–91, 1962.
9. **Johansson B, Lundgren O, and Mellander S.** Reflex influence of "somatic pressor and depressor afferents" on resistance and capacitance vessels and on transcapillary fluid exchange. *Acta Physiol Scand* 62: 280–286, 1964.
10. **Kawada T, Shishido T, Inagaki M, Zheng C, Yanagiya Y, Uemura K, Sugimachi M, and Sunagawa K.** Estimation of baroreflex gain using a baroreflex equilibrium diagram. *Jpn J Physiol* 52: 21–29, 2002.
11. **Kent BB, Drane JW, Blumenstein B, and Manning JW.** A mathematical model to assess changes in the baroreceptor reflex. *Cardiology* 57: 295–310, 1972.
12. **Ku YH and Chang YZ.** β-Endorphin- and GABA-mediated depressor effect of specific electroacupuncture surpasses pressor response of emotional circuit. *Peptides* 22: 1465–1470, 2001.
13. **Ku YH and Zou CJ.** Beta-endorphinergic neurons in nucleus arcuatus and nucleus tractus solitarii mediated depressor-bradycardia effect of "Tinggong" 2-Hz electroacupuncture. *Acupunct Electrother Res* 18: 175–184, 1993.
14. **Legramante JM, Raimondi G, Adreani CM, Sacco S, Iellamo F, Peruzzi G, and Kaufman MP.** Group III muscle afferents evoke reflex depressor responses to repetitive muscle contractions in rabbits. *Am J Physiol Heart Circ Physiol* 278: H871–H877, 2000.
15. **Li L, Yin-Xiang C, Hong X, Peng L, and Da-Nian Z.** Nitric oxide in vPAG mediates the depressor response to acupuncture in stress-induced hypertensive rats. *Acupunct Electrother Res* 26: 165–170, 2001.
16. **Li P.** The effect of acupuncture on blood pressure: the interrelation of sympathetic activity and endogenous opeoid peptides. *Acupunct Electrother Res* 8: 45–56, 1983.
17. **Li P, Pitsillides KF, Rendig SV, Pan HL, and Longhurst JC.** Reversal of reflex-induced myocardial ischemia by median nerve stimulation: a feline model of electroacupuncture. *Circulation* 97: 1186–1194, 1998.
18. **Li P, Rowshan K, Crisostomo M, Tjen-A-Looi SC, and Longhurst JC.** Effect of electroacupuncture on pressor reflex during gastric distension. *Am J Physiol Regul Integr Comp Physiol* 283: R1335–R1345, 2002.
19. **Li P, Tjen-A-Looi S, and Longhurst JC.** Rostral ventrolateral medullary opioid receptor subtypes in the inhibitory effect of electroacupuncture on reflex autonomic response in cats. *Auton Neurosci* 89: 38–47, 2001.
20. **Lin JG, Chang SL, and Cheng JT.** Release of beta-endorphin from adrenal gland to lower plasma glucose by the electroacupuncture at Zhongwan acupoint in rats. *Neurosci Lett* 326: 17–20, 2002.
21. **Lin JG, Lo MW, Wen YR, Hsieh CL, Tsai SK, and Sun WZ.** The effect of high and low frequency electroacupuncture in pain after lower abdominal surgery. *Pain* 99: 509–514, 2002.
22. **Middlekauff HR, Yu JL, and Hui K.** Acupuncture effects on reflex responses to mental stress in humans. *Am J Physiol Regul Integr Comp Physiol* 280: R1462–R1468, 2001.
23. **Mohrman DE and Heller LJ.** *Cardiovascular Physiology* (4th ed.). New York: McGraw-Hill, 1997, p. 158–230.
24. **Moore PG, Quail AW, Cottee DB, McIlveen SA, and White SW.** Effect of fentanyl on baroreflex control of circumflex coronary conductance. *Clin Exp Pharmacol Physiol* 27: 1028–1033, 2000.
25. **Mori H, Uchida S, Ohsawa H, Noguchi E, Kimura T, and Nishijo K.** Electro-acupuncture stimulation to a hindpaw and a hind leg produces different reflex responses in sympathoadrenal medullary function in anesthetized rats. *J Auton Nerv Syst* 79: 93–98, 2000.
26. **Nishijo K, Mori H, Yosikawa K, and Yazawa K.** Decreased heart rate by acupuncture stimulation in humans via facilitation of cardiac vagal activity and suppression of cardiac sympathetic nerve. *Neurosci Lett* 227: 165–168, 1997.
27. **Ohsawa H, Okada K, Nishijo K, and Sato Y.** Neural mechanism of depressor responses of arterial pressure elicited by acupuncture-like stimulation to a hindlimb in anesthetized rats. *J Auton Nerv Syst* 51: 27–35, 1995.
28. **Ohsawa H, Yamaguchi S, Ishimaru H, Shimura M, and Sato Y.** Neural mechanism of pupillary dilation elicited by electro-acupuncture stimulation in anesthetized rats. *J Auton Nerv Syst* 64: 101–106, 1997.
29. **Petty MA and Reid JL.** The effect of opiates on arterial baroreceptor reflex function in the rabbit. *Naunyn Schmiedebergs Arch Pharmacol* 319: 206–211, 1982.
30. **Richter A, Herlitz J, and Hjalmarson A.** Effect of acupuncture in patients with angina pectoris. *Eur Heart J* 12: 175–178, 1991.
31. **Sato T, Kawada T, Inagaki M, Shishido T, Takaki H, Sugimachi M, and Sunagawa K.** New analytic framework for understanding sympathetic baroreflex control of arterial pressure. *Am J Physiol Heart Circ Physiol* 276: H2251–H2261, 1999.
32. **Si QM, Wu GC, and Cao XD.** Effects of electroacupuncture on acute cerebral infarction. *Acupunct Electrother Res* 23: 117–124, 1998.
33. **Sved AF, Ito S, and Madden CJ.** Baroreflex dependent and independent roles of the caudal ventrolateral medulla in cardiovascular regulation. *Brain Res Bull* 51: 129–133, 2000.
34. **Tam KC and Yiu HH.** The effect of acupuncture on essential hypertension. *Am J Chin Med* 3: 369–375, 1975.
35. **Taneyama C, Goto H, Kohno N, Benson KT, Sasao J, and Arakawa K.** Effects of fentanyl, diazepam, and the combination of both on arterial baroreflex and sympathetic nerve activity in intact and baro-denervated dogs. *Anesth Analg* 77: 44–48, 1993.
36. **Tjen-A-Looi SC, Li P, and Longhurst JC.** Prolonged inhibition of rostral ventral lateral medullary premotor sympathetic neurons by electroacupuncture in cats. *Auton Neurosci* 106: 119–131, 2003.

37. **Tjen-A-Looi SC, Peng L, and Longhurst JC.** Medullary substrate and differential cardiovascular responses during stimulation of specific acupoints. *Am J Physiol Regul Integr Comp Physiol* 287: R852–R862, 2004.
38. **Wang JD, Kuo TB, and Yang CC.** An alternative method to enhance vagal activities and suppress sympathetic activities in humans. *Auton Neurosci* 100: 90–95, 2002.
39. **Wong AM, Leong CP, Su TY, Yu SW, Tsai WC, and Chen CP.** Clinical trial of acupuncture for patients with spinal cord injuries. *Am J Phys Med Rehabil* 82: 21–27, 2003.
40. **Wong AM, Su TY, Tang FT, Cheng PT, and Liaw MY.** Clinical trial of electrical acupuncture on hemiplegic stroke patients. *Am J Phys Med Rehabil* 78: 117–122, 1999.
41. **Yamamoto K, Kawada T, Kamiya A, Takaki H, Miyamoto T, Sugimachi M, and Sunagawa K.** Muscle mechanoreflex induces the pressor response by resetting the arterial baroreflex neural arc. *Am J Physiol Heart Circ Physiol* 286: H1382–H1388, 2004.
42. **Yao T.** Acupuncture and somatic nerve stimulation: mechanism underlying effects on cardiovascular and renal activities. *Scand J Rehabil Med Suppl* 29: 7–18, 1993.

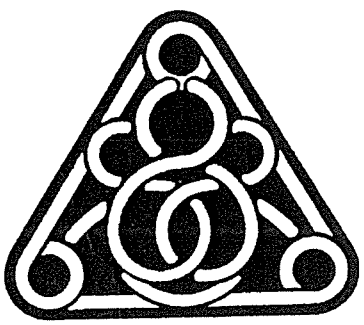

Am J Physiol Heart Circ Physiol 291: H2187–H2191, 2006.
First published June 9, 2006; doi:10.1152/ajpheart.00175.2006.

Effects of Ca^{2+} channel antagonists on nerve stimulation-induced and ischemia-induced myocardial interstitial acetylcholine release in cats

Toru Kawada,[1] Toji Yamazaki,[2] Tsuyoshi Akiyama,[2] Kazunori Uemura,[1] Atsunori Kamiya,[1] Toshiaki Shishido,[1] Hidezo Mori,[2] and Masaru Sugimachi[1]

[1]*Department of Cardiovascular Dynamics, Advanced Medical Engineering Center, National Cardiovascular Center Research Institute and* [2]*Department of Cardiac Physiology, National Cardiovascular Center Research Institute, Osaka, Japan*

Submitted 17 February 2006; accepted in final form 7 June 2006

Kawada, Toru, Toji Yamazaki, Tsuyoshi Akiyama, Kazunori Uemura, Atsunori Kamiya, Toshiaki Shishido, Hidezo Mori, and Masaru Sugimachi. Effects of Ca^{2+} channel antagonists on nerve stimulation-induced and ischemia-induced myocardial interstitial acetylcholine release in cats. *Am J Physiol Heart Circ Physiol* 291: H2187–H2191, 2006. First published June 9, 2006; doi:10.1152/ajpheart.00175.2006.—Although an axoplasmic Ca^{2+} increase is associated with an exocytotic acetylcholine (ACh) release from the parasympathetic postganglionic nerve endings, the role of voltage-dependent Ca^{2+} channels in ACh release in the mammalian cardiac parasympathetic nerve is not clearly understood. Using a cardiac microdialysis technique, we examined the effects of Ca^{2+} channel antagonists on vagal nerve stimulation- and ischemia-induced myocardial interstitial ACh releases in anesthetized cats. The vagal stimulation-induced ACh release [22.4 nM (SD 10.6), $n = 7$] was significantly attenuated by local administration of an N-type Ca^{2+} channel antagonist ω-conotoxin GVIA [11.7 nM (SD 5.8), $n = 7$, $P = 0.0054$], or a P/Q-type Ca^{2+} channel antagonist ω-conotoxin MVIIC [3.8 nM (SD 2.3), $n = 6$, $P = 0.0002$] but not by local administration of an L-type Ca^{2+} channel antagonist verapamil [23.5 nM (SD 6.0), $n = 5$, $P = 0.758$]. The ischemia-induced myocardial interstitial ACh release [15.0 nM (SD 8.3), $n = 8$] was not attenuated by local administration of the L-, N-, or P/Q-type Ca^{2+} channel antagonists, by inhibition of Na^+/Ca^{2+} exchange, or by blockade of inositol 1,4,5-trisphosphate [Ins(1,4,5)P_3] receptor but was significantly suppressed by local administration of gadolinium [2.8 nM (SD 2.6), $n = 6$, $P = 0.0283$]. In conclusion, stimulation-induced ACh release from the cardiac póstganglionic nerves depends on the N- and P/Q-type Ca^{2+} channels (with a dominance of P/Q-type) but probably not on the L-type Ca^{2+} channels in cats. In contrast, ischemia-induced ACh release depends on nonselective cation channels or cation-selective stretch activated channels but not on L-, N-, or P/Q type Ca^{2+} channels, Na^+/Ca^{2+} exchange, or Ins(1,4,5)P_3 receptor-mediated pathway.

cardiac microdialysis; ω-conotoxin GVIA; ω-conotoxin MVIIC; KB-R7943; verapamil; vagal stimulation

ALTHOUGH N-TYPE Ca^{2+} CHANNELS play a dominant role in norepinephrine release from sympathetic nerve endings (8, 33, 34), the type(s) of Ca^{2+} channels controlling ACh release in the mammalian parasympathetic system is not fully understood and show diversity among reports. To name a few, in isolated parasympathetic submandibular ganglia from the rat, neurotransmission is mediated by Ca^{2+} channels that are resistant to the L-, N-, P/Q-, and R- type Ca^{2+} channel antagonists (29). When the negative inotropic response to field stimulation was examined in the isolated guinea pig atria, Hong and Chang (8) reported the importance of P/Q-type Ca^{2+} channels, whereas Serone et al. (28) reported the importance of N-type Ca^{2+} channels. Because field stimulation in the isolated preparations could induce responses different from those in the in vivo conditions, we aimed to examine the effects of Ca^{2+} channel antagonists on the vagal nerve stimulation-induced myocardial interstitial ACh release in the in vivo feline heart.

Aside from the important role of the normal physiological regulation of the heart, the vagal nerve can be a therapeutic target for certain cardiovascular diseases (2, 3, 13, 22, 27). In previous studies, we have shown that acute myocardial ischemia causes myocardial interstitial ACh release in the ischemic region independently of efferent vagal nerve activity (12, 14). The comparison of the effects of Ca^{2+} channel antagonists on the ACh releases induced by vagal nerve stimulation and by acute myocardial ischemia may deepen our understanding about the ischemia-induced myocardial interstitial ACh release.

A cardiac microdialysis technique offers detailed analyses of in vivo myocardial interstitial ACh release (1, 15). Because the local administration of pharmacological agents through a dialysis probe can modulate ACh release without significantly affecting systemic hemodynamics, a combination of cardiac microdialysis with local pharmacological interventions is useful for analyzing the mechanisms of ACh release in vivo. In the present study, we examined the effects of Ca^{2+} channel antagonists on nerve stimulation- and ischemia-induced ACh releases in anesthetized cats. The results indicate that stimulation-induced ACh release from the cardiac parasympathetic postganglionic nerves depends on the N- and P/Q-type Ca^{2+} channels but probably not on the L-type Ca^{2+} channels. In contrast, ischemia-induced myocardial interstitial ACh release is resistant to the inhibition of L-, N-, and P/Q-type Ca^{2+} channels. In addition, the ischemia-induced myocardial ACh release is resistant to the inhibition of Na^+/Ca^{2+} exchanger and the blockade of inositol 1,4,5-trisphosphate [Ins(1,4,5)P_3] receptor but is suppressed by gadolinium, suggesting that nonselective cation channels or cation-selective stretch-activated channels are involved.

MATERIALS AND METHODS

Common Preparation

Animal care was provided in accordance with the *Guiding Principles for the Care and Use of Animals in the Field of Physiological*

Address for reprint requests and other correspondence: T. Kawada, Dept. of Cardiovascular Dynamics, Advanced Medical Engineering Center, National Cardiovascular Center Research Institute, 5-7-1 Fujishirodai, Suita, Osaka 565-8565, Japan (e-mail: torukawa@res.ncvc.go.jp).

The costs of publication of this article were defrayed in part by the payment of page charges. The article must therefore be hereby marked "*advertisement*" in accordance with 18 U.S.C. Section 1734 solely to indicate this fact.

0363-6135/06 $8.00 Copyright © 2006 the American Physiological Society

Sciences approved by the Physiological Society of Japan. All protocols were approved by the Animal Subjects Committee of the National Cardiovascular Center. Adult cats weighing from 2.2 to 4.2 kg were anesthetized via an intraperitoneal injection of pentobarbital sodium (30–35 mg/kg) and ventilated mechanically with room air mixed with oxygen. The depth of anesthesia was maintained with a continuous intravenous infusion of pentobarbital sodium (1–2 $mg \cdot kg^{-1} \cdot h^{-1}$) through a catheter inserted from the right femoral vein. Systemic arterial pressure was monitored from a catheter inserted from the right femoral artery. The vagi were sectioned bilaterally at the neck. The esophageal temperature of the animal, which was measured by a thermometer (CTM-303, TERUMO, Japan), was maintained at around 37°C using a heated pad and a lamp.

With the animal in the lateral position, the left fifth and sixth ribs were resected to expose the heart. A dialysis probe was implanted transversely, using a fine guiding needle, into the anterolateral free wall of the left ventricle perfused by the left anterior descending coronary artery (LAD). Heparin sodium (100 U/kg) was administered intravenously to prevent blood coagulation. At the end of the experiment, the experimental animals were killed with an overdose of pentobarbital sodium. Postmortem examination confirmed that the dialysis probe had been threaded in the middle layer of the left ventricular myocardium. The thickness of the left ventricular free wall was ~7–8 mm, and the semipermeable membrane of the dialysis probe was positioned ~3–4 mm from the epicardial surface.

Dialysis Technique

The materials and properties of the dialysis probe have been described previously (1). Briefly, we designed a transverse dialysis probe. A dialysis fiber of semipermeable membrane (13 mm length, 310 μm OD, 200 μm ID; PAN-1200, 50,000 molecular weight cutoff, Asahi Chemical, Japan) was glued at both ends to polyethylene tubes (25 cm length, 500 μm OD, 200 μm ID). The dialysis probe was perfused at a rate of 2 μl/min with Ringer solution containing a cholinesterase inhibitor eserine (physostigmine, 100 μM). Experimental protocols were started 2 h after the dialysis probe was implanted when the ACh concentration in the dialysate reached a steady state. The ACh concentration in the dialysate was measured by high-performance liquid chromatography with electrochemical detection (Eicom, Kyoto, Japan).

Local administration of a pharmacological agent was carried out through a dialysis probe. That is to say, we added the pharmacological agent to the perfusate and allowed 1 h for a settling time. The pharmacological agent should spread around the semipermeable membrane, thereby affecting the neurotransmitter release in the vicinity of the semipermeable membrane. Because the distribution across the semipermeable membrane is required, based on previous results (33, 34), we used the pharmacological agent at the concentration 10–100 times higher than that required for complete channel blockade in experimental settings in vitro.

Specific Preparation and Protocols

Protocol 1. Bipolar platinum electrodes were attached bilaterally to the cardiac ends of the sectioned vagi at the neck. The nerves and electrodes were covered with warmed mineral oil for insulation. The vagal nerves were stimulated for 15 min (20 Hz, 1 ms, 10 V). We measured the stimulation-induced ACh release in the absence of Ca^{2+} channel blockade (control, $n = 7$) and examined the effects of an L-type Ca^{2+} channel antagonist verapamil (100 μM, $n = 5$), an N-type Ca^{2+} channel antagonist ω-conotoxin GVIA (10 μM, $n = 7$), a P/Q-type Ca^{2+} channel antagonist ω-conotoxin MVIIC (10 μM, $n = 6$), and combined administration of ω-conotoxin GVIA and ω-conotoxin MVIIC (10 μM each, $n = 6$).

Protocol 2. Because a preliminary result from *protocol 1* suggested that local administration of verapamil was ineffective in suppressing stimulation-induced ACh release, we examined the effects of the intravenous administration of verapamil (300 μg/kg, $n = 6$) on stimulation-induced ACh release in vagotomized animals as a supplemental experiment.

Protocol 3. A 60-min LAD occlusion was performed by using a 3-0 silk suture passed around the LAD just distal to the first diagonal branch. We measured the ACh levels during 45–60 min of ischemia in the absence of Ca^{2+} channel blockade (control, $n = 8$) and examined the effects of verapamil (100 μM, $n = 5$), ω-conotoxin GVIA (10 μM, $n = 5$), and ω-conotoxin MVIIC (10 μM, $n = 5$). A previous result indicated that the ischemia-induced ACh release reached the steady state during 45–60 min of ischemia (14). We also examined the effects of three additional agents, a Na^+/Ca^{2+} exchange inhibitor KB-R7943 (10 μM, $n = 5$) (9, 10), an $Ins(1,4,5)P_3$ receptor blocker xestospongin C (500 μM, $n = 6$) (25), and a nonselective cation channel blocker or a cation-selective stretch activated channel blocker gadolinium (1 mM) (5, 17), on the ischemia-induced ACh release.

Statistical Analysis

All data are presented as mean (SD) values. In *protocol 1*, we compared stimulation-induced ACh release among the five groups using one-way analysis of variance followed by the Student-Neuman-Keuls test (6). In *protocol 2*, we used an unpaired-*t* test (two-sided) to examine the effect of intravenous verapamil administration on stimulation-induced ACh release. In *protocol 3*, we compared ischemia-induced ACh release among the seven groups using one-way analysis of variance followed by the Dunnett' test against the control. For all analyses, differences were considered significant when $P < 0.05$.

RESULTS

In *protocol 1*, the ACh level during electrical vagal stimulation was 22.4 nM (SD 10.6). Local administration of verapamil did not affect stimulation-induced ACh release (Fig. 1). In contrast, local administration of ω-conotoxin GVIA or ω-conotoxin MVIIC suppressed stimulation-induced ACh release. The extent of suppression was greater in the latter. The ACh level was significantly lower in the simultaneous administration group (ω-conotoxin GVIA + ω-conotoxin MVIIC)

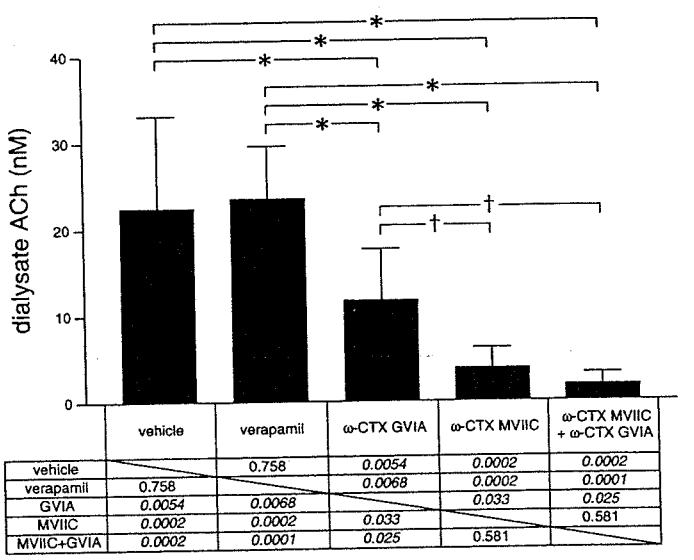

	vehicle	verapamil	ω-CTX GVIA	ω-CTX MVIIC	ω-CTX MVIIC + ω-CTX GVIA
vehicle		0.758	0.0054	0.0002	0.0002
verapamil	0.758		0.0068	0.0002	0.0001
GVIA	0.0054	0.0068		0.033	0.025
MVIIC	0.0002	0.0002	0.033		0.581
MVIIC+GVIA	0.0002	0.0001	0.025	0.581	

Fig. 1. Effects of local administration of verapamil, ω-conotoxin GVIA, ω-conotoxin MVIIC, or ω-conotoxin GVIA plus ω-conotoxin MVIIC on vagal nerve stimulation-induced myocardial interstitial ACh release. Both ω-conotoxin GVIA and ω-conotoxin MVIIC, but not verapamil, suppressed stimulation-induced ACh release. Data are mean (SD) values. *$P < 0.01$, †$P < 0.05$. The exact P values are presented.

than that in the ω-conotoxin GVIA group but was not different from the ω-conotoxin MVIIC group.

In *protocol 2*, the intravenous administration of verapamil did not significantly change stimulation-induced ACh release [21.7 nM (SD 12.8)] compared with the control group (P = 0.91).

In *protocol 3*, the ACh level in the ischemic region was 14.9 nM (SD 8.3) during 45–60 min of acute myocardial ischemia. Inhibition of voltage-dependent Ca^{2+} channels by local administration of verapamil, ω-conotoxin GVIA, or ω-conotoxin MVIIC did not affect ischemia-induced ACh release (Fig. 2). Inhibition of the reverse mode action of Na^+/Ca^{2+} exchange by local administration of KB-R7943 appeared to have augmented rather than suppressed ischemia-induced ACh release, though there was no statistically significant difference from the control. Blockade of the Ins(1,4,5)P_3 receptor by local administration of xestospongin C did not affect the ischemia-induced ACh release. In contrast, blockade of nonselective cation channels or cation-selective stretch-activated channels by local administration of gadolinium suppressed the ischemia-induced ACh release.

DISCUSSION

Ca^{2+} Channels Involved in Stimulation-Induced ACh Release

Although neurotransmitter release at mammalian sympathetic neuroeffector junctions predominantly depends on Ca^{2+} influx through N-type Ca^{2+} channels (23, 33, 34), the type(s) of Ca^{2+} channels involved in ACh release from cardiac parasympathetic neuroeffector junctions show diversity among reports (8, 28). One possible factor hampering investigations into parasympathetic postganglionic neurotransmitter release in response to vagal nerve stimulation in vivo is that the parasympathetic ganglia are usually situated in the vicinity of the effector organs, thereby making it difficult to separately assess ACh release from preganglionic and postganglionic nerves. In the previous study from our laboratory, intravenous administration, but not local administration of a ganglionic blocker, hexamethonium reduced vagal stimulation-induced ACh release assessed by cardiac microdialysis (1). The negligible effect of local hexamethonium administration on stimulation-induced ACh release suggests the lack of parasympathetic ganglia around the dialysis probe. In support of our speculation, a recent neuroanatomical finding indicates that three ganglia, away from the left anterior free wall targeted by the dialysis probe, provide the major source for left ventricular postganglionic innervation in cats: a cranioventricular ganglion, a left ventricular ganglion 2 (so designated), and an interventriculo-septal ganglion (11). Therefore, ACh, as measured by cardiac microdialysis, is considered to predominantly reflect ACh release from parasympathetic postganglionic nerves.

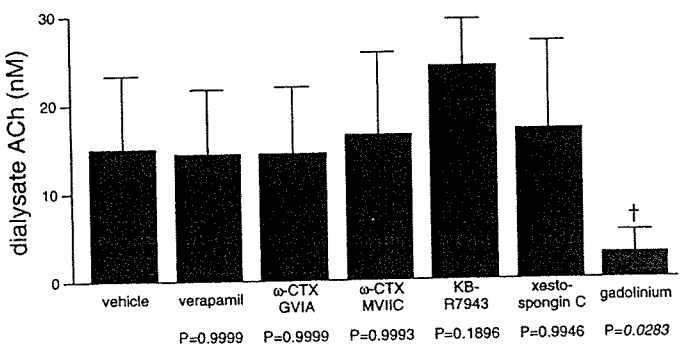

Fig. 2. Effects of local administration of verapamil, ω-conotoxin GVIA, ω-conotoxin MVIIC, KB-R7943, xestospongin C, or gadolinium on acute myocardial ischemia-induced myocardial interstitial ACh release in the ischemic region. Gadolinium alone suppressed the ischemia-induced ACh release. Data are mean (SD) values. †$P < 0.05$. The exact P values are presented.

Local (*protocol 1*) or intravenous (*protocol 2*) administration of verapamil did not affect stimulation-induced ACh release. In contrast, vagal stimulation-induced ACh release was reduced in both the ω-conotoxin GVIA and ω-conotoxin MVIIC groups but to a greater extent in the latter (Fig. 1). Therefore, both N- and P/Q-type, but probably not L-type, Ca^{2+} channels are involved in stimulation-induced ACh release from the cardiac parasympathetic postganglionic nerves in cats. The contribution of P/Q type Ca^{2+} channels to ACh release might be greater than that of N-type Ca^{2+} channels. Hong and Chang (8) reported that the negative inotropic response to field stimulation depends predominantly on the P/Q-type Ca^{2+} channels in isolated guinea pig atria, whereas Serone et al. (28) reported the predominance of N-type Ca^{2+} channels. In those studies, the field stimulation employed differed from ordinary activation of the postganglonic nerves by nerve discharge and, in addition, ACh release was not directly measured. The present study directly demonstrated the involvement of P/Q- and N-type Ca^{2+} channels in the stimulation-induced ACh release in the cardiac parasympathetic postganglionic nerves. These results support the concept that multiple subtypes of the voltage-gated Ca^{2+} channel mediate transmitter release from the same population of parasympathetic neurons (31).

Stimulation-induced ACh release was suppressed by ~50% in the ω-conotoxin GVIA group and by ~80% in the ω-conotoxin MVIIC group. The algebraic summation of the extent of suppression exceeded 100%. The phenomenon may be in part due to the nonlinear dose-response relationship between Ca^{2+} influx and transmitter release (32). The supra-additive phenomenon may be also due to the affinity of ω-conotoxin MVIIC to N-type Ca^{2+} channels (8, 26, 36). Combined local administration of ω-conotoxin GVIA and ω-conotoxin MVIIC almost completely suppressed stimulation-induced ACh release to a level similar to that achieved by the Na^+ channel inhibitor tetrodotoxin (15). Therefore, involvement of another untested type of Ca^{2+} channel(s) is unlikely in the stimulation-induced ACh release from the cardiac parasympathetic postganglionic nerves in cats.

Ca^{2+} Channels and Ischemia-Induced ACh Release

In a previous study, we showed that acute myocardial ischemia evokes myocardial interstitial ACh release in the ischemic region via a local mechanism independent of efferent vagal nerve activity (14). In that study, the inhibition of intracellular Ca^{2+} mobilization by local administration of 3,4,5-trimethoxybenzoic acid 8-(diethyl amino)-octyl ester (TMB-8) suppressed ischemia-induced ACh release, suggesting that an axoplasmic Ca^{2+} elevation is essential for the ischemia-induced ACh release. Because tissue K^+ concentration increases in the ischemic region (7, 18), high K^+-induced

depolarization could activate voltage-dependent Ca^{2+} channels even in the absence of efferent vagal nerve activity. However, ischemia-induced ACh release was not suppressed by local administration of verapamil, ω-conotoxin GVIA, or ω-conotoxin MVIIC (Fig. 2). Therefore, Ca^{2+} entry through the voltage-dependent Ca^{2+} channels is unlikely a mechanism for the ischemia-induced myocardial interstitial ACh release.

Acute myocardial ischemia causes energy depletion in the ischemic region, which impairs Na^+-K^+-ATPase activity. Ischemia also causes acidosis in the ischemic region, which promotes Na^+/H^+ exchange. As a result, ischemia causes intracellular Na^+ accumulation. The decrease in the Na^+ gradient across the plasma membrane may then cause the Na^+/Ca^{2+} exchanger to operate in the reverse mode, facilitating intracellular Ca^{2+} overload. KB-R7943 can inhibit the reverse mode of Na^+/Ca^{2+} exchange (9, 10) and its potential to protect against ischemia-reperfusion injury has been reported (21). In the present study, however, local administration of KB-R7943 failed to suppress and rather increased ACh release during ischemia as opposed to our expectation. It is plausible that the inhibition of reverse mode of Na^+/Ca^{2+} may have facilitated the accumulation of intracellular Na^+ and induced adverse effects that cancelled the possible beneficial effects derived from the inhibition of Ca^{2+} entry through the Na^+/Ca^{2+} exchanger itself. In addition, KB-R7943 could inhibit the forward mode of Na^+/Ca^{2+} exchange and reduce Ca^{2+} efflux (16), contributing to the intracellular Ca^{2+} accumulation and ACh release. In the present study, we observed the effects of KB-R7943 only during the ischemic period. However, accumulation of intracellular Na^+ through Na^+/H^+ exchange is enhanced on reperfusion due to the washout of extracellular H^+ (20). The inhibition of Na^+/Ca^{2+} exchange to suppress Ca^{2+} overload might become more important during the reperfusion phase. For instance, the percent segment shortening of the left ventricle was improved by KB-R7943 during reperfusion but not during ischemia (35).

As already mentioned, the ischemia-induced ACh release can be blocked by TMB-8 and thus the intracellular Ca^{2+} mobilization is required for the ischemia-induced ACh release (14). Besides the Ca^{2+} entries through voltage-dependent Ca^{2+} channels and via the reverse mode of Na^+/Ca^{2+} exchanger, Ca^{2+} may be mobilized from the endoplasmic reticulum via pathological pathways. As an example, the mitochondrial permeability transition pore triggered in pathological conditions is linked to cytochrome *c* release. Cytochrome *c* can bind to the endoplasmic reticulum $Ins(1,4,5)P_3$ receptor, rendering the channel insensitive to autoinhibition by high cytosolic Ca^{2+} concentration and resulting in enhanced endoplasmic reticulum Ca^{2+} release (4, 30). In the present study, however, blockade of $Ins(1,4,5)P_3$ receptor by xestospongin C failed to suppress the ischemia-induced ACh release. In contrast, local administration of gadolinium significantly suppressed the ischemia-induced ACh release. Therefore, nonselective cation channels or cation-selective stretch-activated channels contribute to the ischemia-induced ACh release. During myocardial ischemia, the ischemic region can be subjected to paradoxical systolic bulging. Such bulging likely opens stretch-activated channels and causes myocardial interstitial ACh release, possibly leading to cardioprotection by ACh against ischemic injury (2).

Limitations

First, the experiment was performed under anesthetic conditions, which may have influenced basal autonomic activity. However, because we sectioned the vagi at the neck, basal autonomic activity may have had only a minor effect on ACh release during the vagal stimulation and during acute myocardial ischemia. Second, we added eserine to the perfusate to inhibit immediate degradation of ACh (24), which may have increased the ACh level in the synaptic cleft and activated regulatory pathways such as autoinhibition of ACh release via muscarinic receptors (24). However, the myocardial interstitial ACh level measured under this condition could reflect changes induced by Na^+ channel inhibitor, choline uptake inhibitor, and vesicular ACh transport inhibitor as described in a previous study (15). Therefore, we think that the interpretation of the present results is reasonable. Third, tissue and species differences should be taken into account when extrapolating the present findings, because significant heterogeneity in the Ca^{2+} channels involved in the mammalian parasympathetic system may exist. Finally, we used verapamil to test the involvement of L-type Ca^{2+} channels in the ACh release. There are three major types of L-type Ca^{2+} channel antagonists with different binding domains (verapamil, nifedipine, and diltiazem) (19). Whether the effects on the ACh release are common among the three types of L-type Ca^{2+} channel antagonists remains unanswered.

In conclusion, the N- and P/Q-type Ca^{2+} channels (with the P/Q-type dominant), but probably not the L-type Ca^{2+} channels, are involved in vagal stimulation-induced ACh release from the cardiac parasympathetic postganglionic nerves in cats. In contrast, myocardial interstitial ACh release in the ischemic myocardium is resistant to the blockade of L-, N-, and P/Q-type Ca^{2+} channels. In addition, the ischemia-induced myocardial ACh release is resistant to the inhibition of Na^+/Ca^{2+} exchanger and the blockade of $Ins(1,4,5)P_3$ receptor but is suppressed by gadolinium, suggesting that nonselective cation channels or cation-selective stretch-activated channels are involved.

GRANTS

This study was supported by Health and Labour Sciences Research Grant for Research on Advanced Medical Technology from the Ministry of Health, Labour and Welfare of Japan, Health and Labour Sciences Research Grant for Research on Medical Devices for Analyzing, Supporting and Substituting the Function of Human Body from the Ministry of Health, Labour and Welfare of Japan, Health and Labour Sciences Research Grant H18-Iryo-Ippan-023 from the Ministry of Health, Labour and Welfare of Japan, Program for Promotion of Fundamental Studies in Health Science from the National Institute of Biomedical Innovation, a Grant provided by the Ichiro Kanehara Foundation, Ground-based Research Announcement for Space Utilization promoted by Japan Space Forum, and Industrial Technology Research Grant Program in 03A47075 from New Energy and Industrial Technology Development Organization of Japan.

REFERENCES

1. **Akiyama T, Yamazaki T, and Ninomiya I.** In vivo detection of endogenous acetylcholine release in cat ventricles. *Am J Physiol Heart Circ Physiol* 266: H854–H860, 1994.
2. **Ando M, Katare RG, Kakinuma Y, Zhang D, Yamasaki F, Muramoto K, and Sato T.** Efferent vagal nerve stimulation protects heart against ischemia-induced arrhythmias by preserving connexin43 protein. *Circulation* 112: 164–170, 2005.

3. **Bibevski S and Dunlap ME.** Prevention of diminished parasympathetic control of the heart in experimental heart failure. *Am J Physiol Heart Circ Physiol* 287: H1780–H1785, 2004.
4. **Brookes PS, Yoon Y, Robotham JL, Anders MW, and Sheu SS.** Calcium, ATP, and ROS: a mitochondrial love-hate triangle. *Am J Physiol Cell Physiol* 287: C817–C833, 2004.
5. **Caldwell RA, Clemo HF, and Baumgarten CM.** Using gadolinium to identify stretch-activated channels: technical considerations. *Am J Physiol Cell Physiol* 275: C619–C621, 1998.
6. **Glantz SA.** *Primer of Biostatistics* (5th ed) New York: McGraw-Hill, 2002.
7. **Hirche HJ, Franz CHR, Bös L, Bissig R, Lang R, and Schramm M.** Myocardial extracellular K^+ and H^+ increase and noradrenaline release as possible cause of early arrhythmias following acute coronary artery occlusion in pigs. *J Mol Cell Cardiol* 12: 579–593, 1979.
8. **Hong SJ and Chang CC.** Calcium channel subtypes for the sympathetic and parasympathetic nerves of guinea-pig atria. *Br J Pharmacol* 116: 1577–1582, 1995.
9. **Iwamoto T, Kita S, Uehara A, Inoue Y, Taniguchi Y, Imanaga I, and Shigekawa M.** Structural domains influencing sensitivity to isothiourea derivative inhibitor KB-R7943 in cardiac Na^+/Ca^{2+} exchanger. *Mol Pharmacol* 59: 524–531, 2001.
10. **Iwamoto T, Watano T, and Shigekawa M.** A novel isothiourea derivative selectively inhibits the reverse mode of Na^+/Ca^{2+} exchange in cells expressing NCX1. *J Biol Chem* 271: 22391–22397, 1996.
11. **Johnson TA, Gray AL, Lauenstein JM, Newton SS, and Massari VJ.** Parasympathetic control of the heart. I. An interventriculo-septal ganglion is the major source of the vagal intracardiac innervation of the ventricles. *J Appl Physiol* 96: 2265–2272, 2004.
12. **Kawada T, Yamazaki T, Akiyama T, Inagaki M, Shishido T, Zheng C, Yanagiya Y, Sugimachi M, and Sunagawa K.** Vagosympathetic interactions in ischemia-induced myocardial norepinephrine and acetylcholine release. *Am J Physiol Heart Circ Physiol* 280: H216–H221, 2001.
13. **Kawada T, Yamazaki T, Akiyama T, Li M, Ariumi H, Mori H, Sunagawa K, and Sugimachi M.** Vagal stimulation suppresses ischemia-induced myocardial interstitial norepinephrine release. *Life Sci* 78: 882–887, 2006.
14. **Kawada T, Yamazaki T, Akiyama T, Sato T, Shishido T, Inagaki M, Takaki H, Sugimachi M, and Sunagawa K.** Differential acetylcholine release mechanisms in the ischemic and non-ischemic myocardium. *J Mol Cell Cardiol* 32: 405–414, 2000.
15. **Kawada T, Yamazaki T, Akiyama T, Shishido T, Inagaki M, Uemura K, Miyamoto T, Sugimachi M, Takaki H, and Sunagawa K.** In vivo assessment of acetylcholine-releasing function at cardiac vagal nerve terminals. *Am J Physiol Heart Circ Physiol* 281: H139–H145, 2001.
16. **Kimura J, Watano T, Kawahara M, Sakai E, and Yatabe J.** Direction-independent block of bi-directional Na^+/Ca^{2+} exchange current by KB-R7943 in guinea-ping cardiac myocytes. *Br J Pharmacol* 128: 969–974, 1999.
17. **Kimura S, Mieno H, Tamaki K, Inoue M, and Chayama K.** Nonselective cation channel as a Ca^{2+} influx pathway in pepsinogen-secreting cells of bullfrog esophagus. *Am J Physiol Gastrointest Liver Physiol* 281: G333–G341, 2001.
18. **Kléber AG.** Extracellular potassium accumulation in acute myocardial ischemia. *J Mol Cell Cardiol* 16: 389–394, 1984.
19. **Kurokawa J, Adachi-Akahane S, and Nagao T.** 1–5-Benzothiazepine binding domain is located on the extracellular side of the cardiac L-type Ca^{2+} channel. *Mol Pharmacol* 51: 262–268, 1997.
20. **Lazdunski M, Frelin C, and Vigne P.** The sodium/hydrogen exchange system in cardiac cells: its biochemical and pharmacological properties and its role in regulating internal concentrations of sodium and internal pH. *J Mol Cell Cardiol* 17: 1029–1042, 1985.
21. **Lee C, Dhalla NS, and Hryshko LV.** Therapeutic potential of novel Na^+-Ca^{2+} exchange inhibitors in attenuating ischemia-reperfusion injury. *Can J Cardiol* 21: 509–516, 2005.
22. **Li M, Zheng C, Sato T, Kawada T, Sugimachi M, and Sunagawa K.** Vagal nerve stimulation markedly improves long-term survival after chronic heart failure in rats. *Circulation* 109: 120–124, 2004.
23. **Molderings GJ, Likungu J, and Göthert M.** N-type calcium channels control sympathetic neurotransmission in human heart atrium. *Circulation* 101: 403–407, 2000.
24. **Nicholls DG.** *Proteins, Transmitters and Synapses*. Oxford: Blackwell Science, 1994.
25. **Oka T, Sato K, Hori M, Ozaki H, and Karaki H.** Xestospongin C, a novel blocker of IP_3 receptor, attenuates the increase in cytosolic calcium level and degranulation that is induced by antigen in RBL-2H3 mast cells. *Br J Pharmacol* 135: 1959–1966, 2002.
26. **Randall A and Tsien RW.** Pharmacological dissection of multiple types of Ca^{2+} channel currents in rat cerebellar granule neurons. *J Neurosci* 15: 2995–3012, 1995.
27. **Schauerte P, Scherlag BJ, Scherlag MA, Goli S, Jackman WM, and Lazzara R.** Ventricular rate control during atrial fibrillation by cardiac parasympathetic nerve stimulation: a transvenous approach. *J Am Coll Cardiol* 34: 2043–2050, 1999.
28. **Serone AP and Angus JA.** Role of N-type calcium channels in autonomic neurotransmission in guinea-pig isolated left atria. *Br J Pharmacol* 127: 927–934, 1999.
29. **Smith AB, Motin L, Lavidis NA, and Adams DJ.** Calcium channels controlling acetylcholine release from preganglionic nerve terminals in rat autonomic ganglia. *Neuroscience* 95: 1121–1127, 2000.
30. **Verkhratsky A and Toescu EC.** Endoplasmic reticulum Ca^{2+} homeostasis and neuronal death. *J Cell Mol Med* 4: 351–361, 2003.
31. **Waterman SA.** Multiple subtypes of voltage-gated calcium channel mediate transmitter release from parasympathetic neurons in the mouse bladder. *J Neurosci* 16: 4155–4161, 1996.
32. **Wheeler DB, Randall A, and Tsien RW.** Changes in action potential duration after reliance of excitatory synaptic transmission on multiple types of Ca^{2+} channels in rat hippocampus. *J Neurosci* 16: 2226–2237, 1996.
33. **Yahagi N, Akiyama T, and Yamazaki T.** Effects of ω-conotoxin GVIA on cardiac sympathetic nerve function. *J Auton Nerv Syst* 68: 43–48, 1998.
34. **Yamazaki T, Akiyama T, Kitagawa H, Takauchi Y, Kawada T, and Sunagawa K.** A new, concise dialysis approach to assessment of cardiac sympathetic nerve terminal abnormalities. *Am J Physiol Heart Circ Physiol* 272: H1182–H1187, 1997.
35. **Yoshitomi O, Akiyama D, Hara T, Cho S, Tomiyasu S, and Sumikawa K.** Cardioprotective effects of KB-R7943, a novel inhibitor of Na^+/Ca^{2+} exchanger, on stunned myocardium in anesthetized dogs. *J Anesth* 19: 124–130, 2005.
36. **Zhang JF, Randall AD, Ellinor PT, Horne WA, Sather WA, Tanabe T, Schwarz TL, and Tsien RW.** Distinctive pharmacology and kinetics of cloned neuronal Ca^{2+} channels and their possible counterparts in mammalian CNS neurons. *Neuropharmacology* 32: 1075–1088, 1993.

バイオニック治療戦略

高知大学循環制御学　佐藤隆幸（さとうたかゆき）
九州大学大学院医学研究院循環器内科学　砂川賢二（すながわけんじ）

はじめに

循環器疾患では，心不全や圧反射失調のように制御機構の機能破綻が病態の悪化や予後を規定する因子になることがある．そこで，積極的に循環制御機構の機能再建や最適化を図るための新しい治療戦略として，神経インターフェイス技法を用いたバイオニック療法が提唱されている[1]．

本稿では迷走神経の電気刺激による心不全治療[2]に関する実験的研究，および脊髄交感神経刺激による術中自動血圧制御に関する臨床研究[3]について紹介する．

迷走神経刺激による慢性心不全治療

最新の病態に関する研究により，慢性心不全の重要な予後規定因子として，循環調節機構の破綻があげられている．当初は，心機能低下の代償機転として適応的にはたらいていた交感神経系の活性化と副交感神経系の活動低下やレニン・アンジオテンシン系の活性化が，次第に心臓リモデリングを進展・悪化させ，一種の悪循環を形成し，最終的には調節破綻に陥ると考えられるようになってきた．さらに，大規模臨床試験により，呼吸性心拍変動の低下や心拍数増加が予後不良因子として認識されるようになった．これらはいずれも心臓迷走神経活動の低下を反映したものである[4~8]．そこで，「迷走神経を電気刺激する神経インターフェイス療法」が生命予後を改善するか否かを心不全モデル動物を用いて実験的に検証した．

左冠動脈起始部の結紮により，左室の40～50％が梗塞に陥った慢性心不全ラットの右迷走神経に刺激電極を固定し，植え込み型電気刺激装置と接続した．刺激強度は心拍数が10～20％低下する程度にした．迷走神経刺激療法は6週間でうち切り，血行動態・心臓リモデリングに与える影響と140日間の長期生存率を観察した．

1.　心機能およびリモデリングに与える影響

図1は治療終了時の血行動態の比較を示している．血圧は，梗塞後心不全群は健常群に比べ有意に低かった．梗塞後心不全群は，健常群に比べ左室拡張末期圧の有意な上昇と左室圧一次微分最大値の有意な低下を示したが，迷走神経刺激療法により，左室拡張末期圧の有意な減少と左室圧一次微分最大値の有意な上昇が認められた．両心室重量が，梗塞後心不全群では有意な増加を示したが，迷走神経刺激療法により有意に減少した．以上の結果は，6週間の迷走神経刺激療法によってポンプ機能が改善し心室リモデリングが予防されたことを示唆する．

[Key words]　循環調節，迷走神経，交感神経，神経インターフェイス

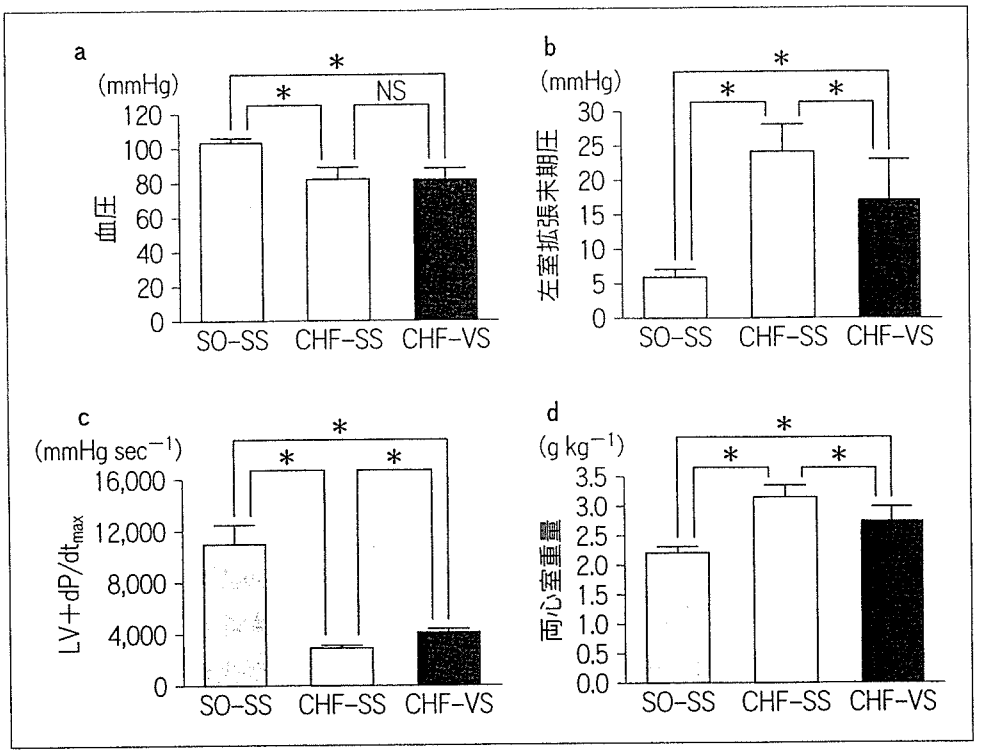

図1　迷走神経刺激の血行動態および両心室重量に与える影響

健常群（SO-SS, $n=9$），梗塞後心不全における非刺激群（CHF-SS, $n=13$）および梗塞後心不全における刺激群（CHF-VS, $n=11$）．数値は平均±標準偏差で示している．$^*p<0.05$.

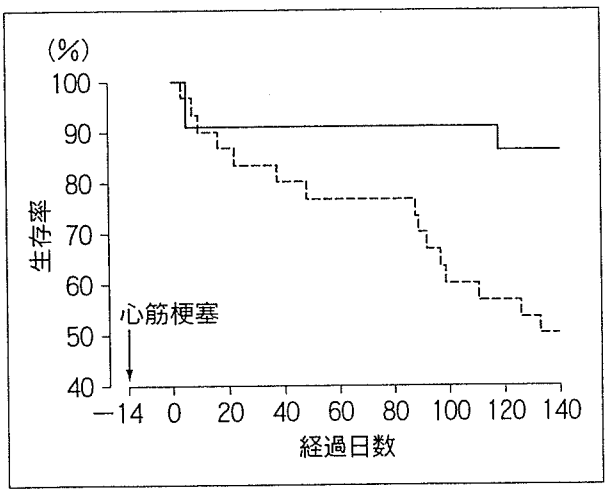

図2　迷走神経刺激の慢性心不全ラットの生存率に与える影響

実線は刺激群（$n=22$），破線は非刺激群（$n=30$）を示す．迷走神経刺激により生存率は有意に改善した（$p=0.008$）．

2.　長期生存率および液性因子に与える影響

迷走神経刺激療法の生存率に与える影響をKaplan-Meier法により解析した．140日の観察期間における生存率曲線を図2に示す．刺激群22例のうち死亡は3例，非刺激群30例のうち死亡は15例であった（$p=0.008$）．このように，迷走神経刺激療法は相対的死亡リスクを73％も減少させた．この効果は，アンジオテンシン変換酵素阻害薬によるものよりもさらに良好な成績であった[9]．

迷走神経刺激療法は，両心室重量，血漿ノルエピネフリンおよび脳性ナトリウム利尿ペプチドを有意に減少させた．なお，これらの指標はいずれも臨床試験で明らかにされている予後規定因子で，高値ほど予後不良とされているものである．

以上より，迷走神経刺激療法が心機能の改善とリモデリングを予防し，さらに，長期予後を著明に改善することが明らかになった[2]．

3.　迷走神経刺激による抗リモデリング機序

迷走神経刺激により，不全心で生ずるリモデリングが予防される機序として，徐脈によりエネル

ギー効率の改善[10]，冠循環における血管内皮機能の改善[11]などが考えられるが，不明なところも多い．最近，筆者らは，迷走神経の末端から放出されるアセチルコリンが心筋細胞に与える影響について調べたところ，アセチルコリンがムスカリン受容体を介して，低酸素誘導因子 HIF-1α の発現を促進し，不全心でみられるアポトーシスを防止する可能性があることを報告した[12]．また，末期心不全における致死性不整脈との関連が示唆されているギャップ結合の機能低下を迷走神経刺激が防止する可能性があることを示した[13]．おもしろいことに，これらの迷走神経あるいはアセチルコリンの心筋細胞に与える効果は，徐脈効果とは独立した機序である可能性がある．

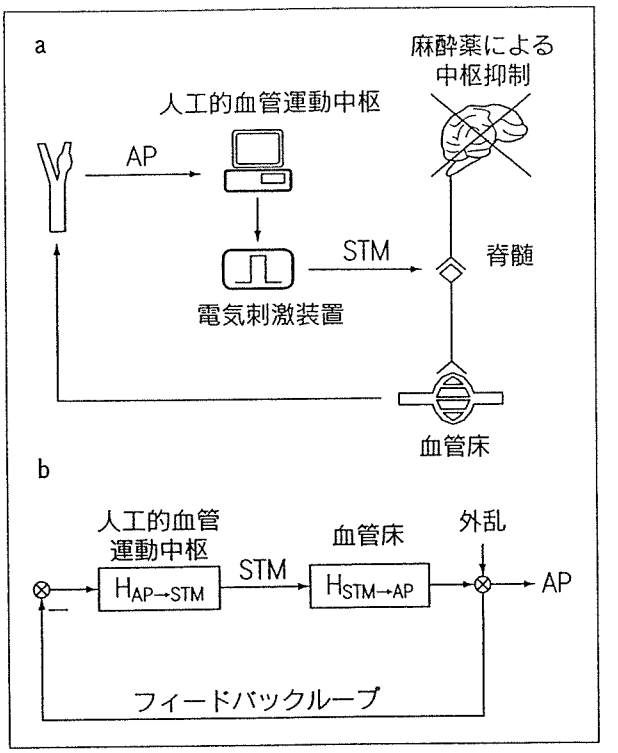

図3　バイオニック圧反射装置
バイオニック圧反射装置の概要（a）とブロック線図（b）．
AP と STM はそれぞれ血圧と電気刺激を示す．

脊髄交感神経刺激による術中血圧の自動制御

動脈圧受容器反射は短期血圧調節にきわめて重要な役割を果たしているが[14,15]，多くの麻酔薬が

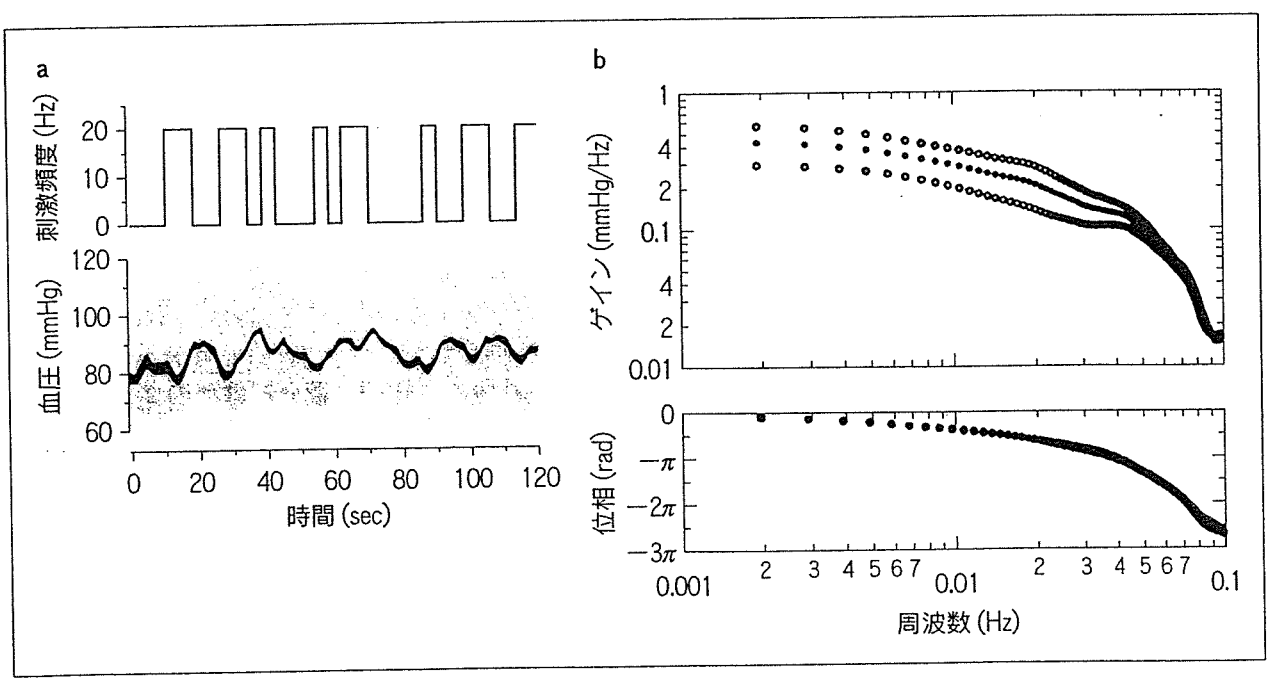

図4　脊髄交感神経の不規則刺激の例と伝達関数
a：不規則な電気刺激に対する血圧の応答は緩徐である．
b：電気刺激に対する血圧応答に関する伝達関数（$n=12$）．伝達関数により刺激に対する動脈圧応答が定量的に推定可能になる．数値は平均(●)±標準偏差(○)で示している．

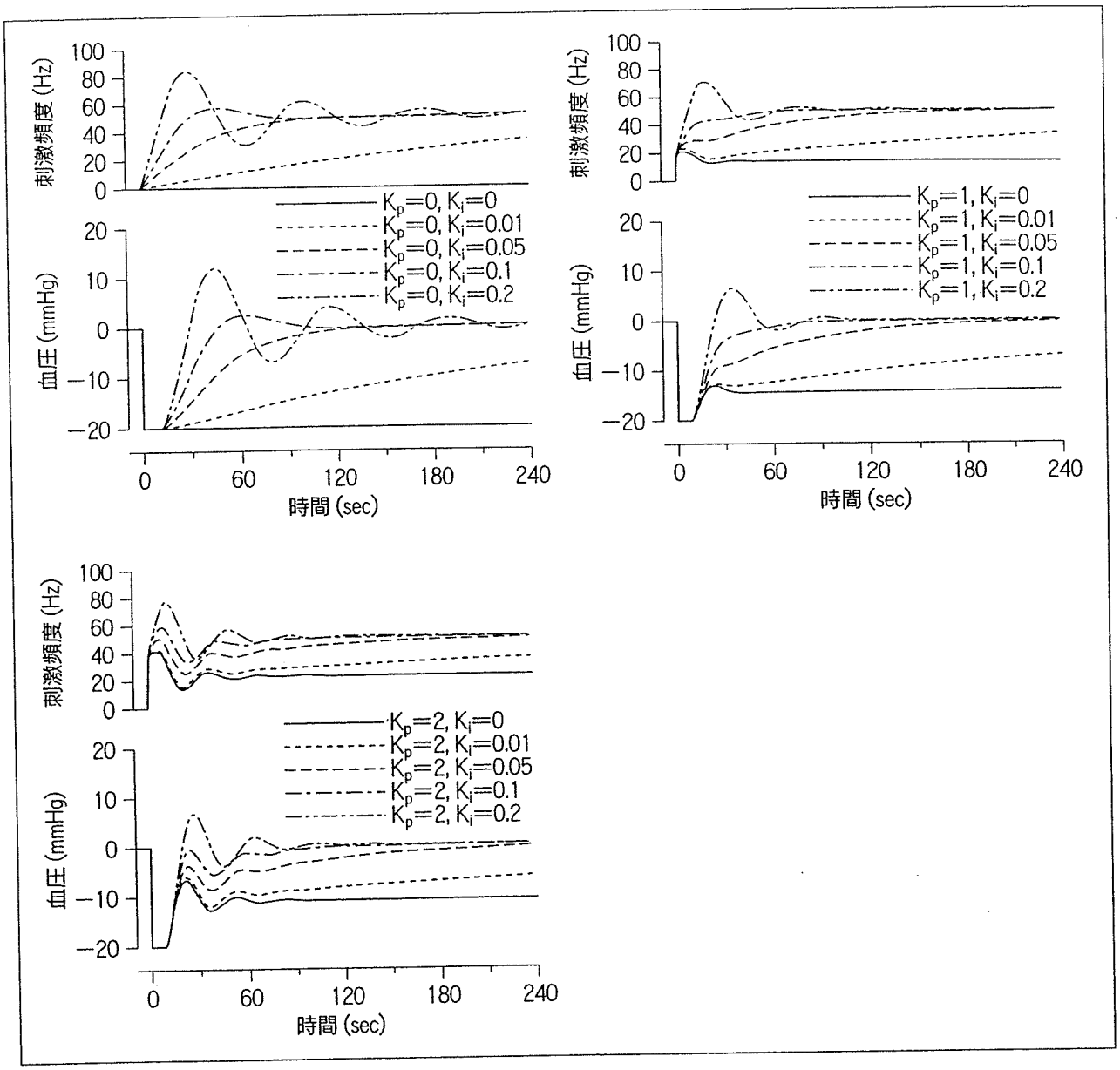

図5　数値シミュレーションによる人工的血管運動中枢の補償係数パラメータの決定
K_p と K_i はそれぞれ，比例補償係数と積分補償係数を示す．

この機能を抑制するため[16,17]，少量の出血などでも予期せぬ血圧低下をきたすことがある[18,19]．そこで，図3のように，圧センサー→コンピュータ→電気刺激装置→硬膜外カテーテル電極を用いたバイオニック圧反射装置 (bionic baroreflex system: BBS) を用いて，血圧の自動制御を試みた．

1.　動作原理の開発戦略

サーボコントロールの原理を応用してBBSを試作した．サーボコントローラの動作原理としては，いわゆる，比例・積分補償型のネガティブフィードバックを採用した[20]．被制御変数である瞬時血圧 $AP(f)$ の標的血圧 $AP_t(f)$ からの偏差，すなわち，制御誤差 $E(f)$ は，$E(f)=AP_t(f)-AP(f)$ と表される．$E(f)$ から脊髄交感神経刺激 $STM(f)$ までの伝達関数 $H_1(f)$ は，比例補償係数 K_p と積分補償係数 K_i および Laplace 演算子 $s=2\pi fj$ を用いると次のように表される．

$$H_1(f)=K_p\frac{K_i}{s}$$

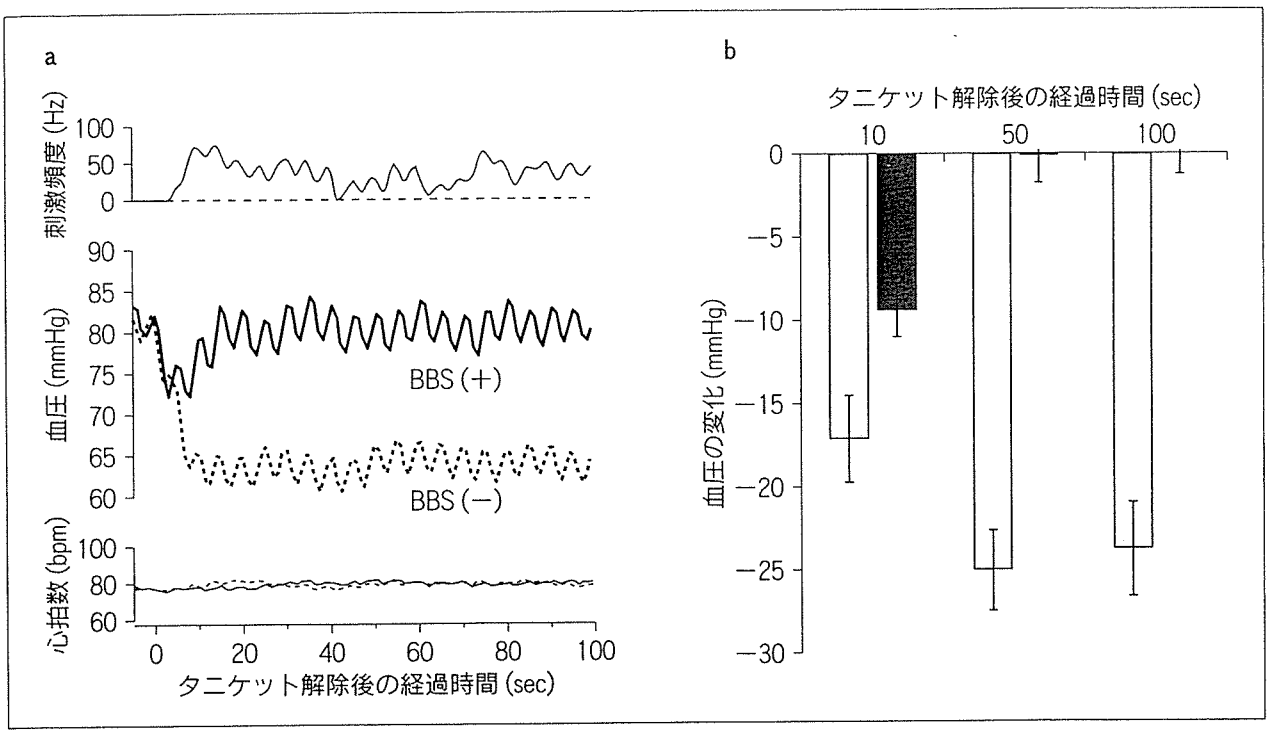

図 6　バイオニック圧反射装置を用いた術中血圧制御

a：典型例.

b：21例における BBS の有効性に関する評価．BBS 未使用の場合（□）と BBS 使用の場合（■）．数値は平均±標準偏差である.

また，脊髄交感神経刺激に対する血圧の応答特性を示す伝達関数を $H_2(f)$ とすると，被制御変数は次のように表される.

$$AP(f)=\frac{H_1(f)H_2(f)}{1+H_1(f)H_2(f)}AP_t(f)+\frac{1}{1+H_1(f)H_2(f)}AP_d(f)$$

ここで，$AP_d(f)$ は，サーボコントロールシステムに加わる外乱である．上の式から明らかなように，外乱の影響は，$1/(1+H_1(f)H_2(f))$ に抑制されることがわかる.

したがって，外乱に抗して血圧の安定化を図るためには，$H_1(f)$ の最適設計が必要である．そこで，まず，計測可能な $H_2(f)$ を次項のような方法で求め，ついで，数値シミュレーションにより $H_1(f)$ の係数 K_p および K_i を最適になるように設計した.

2.　サーボコントローラの設計

頸椎手術症例で，術中に脊髄誘発電位検査を施行予定の患者を対象にした．吸入麻酔薬による全身麻酔の導入後，経皮的に硬膜外カテーテル電極を挿入し，第 9 ないし第12胸椎レベルに電極を留置した．ついで刺激パルスのパラメータをパルス幅0.1ミリ秒，刺激頻度20 Hz に設定した．刺激強度は，この刺激パルスにより平均動脈圧がおおむね10 mmHg だけ上昇する電流値に調整した．筋弛緩薬投与下で，電気刺激装置に白色雑音様の不規則なトリガー信号を入力しながら，動脈圧の変動を15分間記録した．刺激パルスの頻度は，0 か 20 Hz かのいずれかになるように 8 秒間隔ごとに不規則に切り替えた．不規則刺激中の血圧応答の例を図 4a に，また推定された伝達関数 $H_2(f)$ を図 4b に示す．ついで，12例で求めた平均的 $H_2(f)$ を用いて，ステップ状の血圧低下（−20 mmHg）に対する血圧サーボシステムの振る舞いを比例補償係数 $K_p=0, 1, 2$，積分補償係数 $K_i=0, 0.01,$

0.05, 0.1, 0.2の組み合せでシミュレーションした．その結果，$K_p=1$, $K_i=0.1$の場合にもっとも迅速かつ安定的に血圧低下が防止されることが明らかとなった（図5）．そこで，$K_p=1$, $K_i=0.1$として人工的血管運動中枢をプログラムした．

3. BBSの有効性の検証

膝の人工関節置換術時に大腿に巻かれたタニケット（圧迫止血帯）の解除に伴う血圧低下を外乱とみなし，BBSの有効性を検証した．その結果，図6に示すように，BBSを用いることにより迅速で安全な自動血圧管理が可能であることが明らかになった[3]．

まとめ

神経インターフェイス技法に基づいたバイオニック療法が，慢性心不全に対する画期的な治療戦略となりうることを示す基礎研究結果，およびバイオニック圧反射装置により術中血圧を自動管理しうることを示唆する臨床研究結果を得ることができた．積極的に循環調節の破綻を是正したり，機能を再建することにより循環器疾患を治療するというバイオニック戦略の今後の展開に期待したい．

文献

1) Sato T, Kawada T, Sugimachi M et al: Bionic technology revitalizes native baroreflex function in rats with baroreflex failure. Circulation 2002; **106**: 730–734
2) Li M, Zheng C, Sato T et al: Vagal nerve stimulation markedly improves long-term survival after chronic heart failure in rats. Circulation 2004; **109**: 120–124
3) Yamasaki F, Ushida T, Yokoyama T et al: Artificial baroreflex: clinical application of a bionic baroreflex system. Circulation 2006; in press
4) Pfeffer MA: Left ventricular remodeling after acute myocardial infarction. Annu Rev Med 1995; **46**: 455–466
5) Cerati D, Schwartz PJ: Single cardiac vagal fiber activity, acute myocardial ischemia, and risk for sudden death. Circ Res 1991; **69**: 1389–1401
6) Schwartz PJ, La Rovere MT, Vanoli E: Autonomic nervous system and sudden cardiac death. Experimental basis and clinical observations for post-myocardial infarction risk stratification. Circulation 1992; **85**(Suppl I): I-77–I-91
7) La Rovere MT, Bigger JT Jr, Marcus FI et al: Baroreflex sensitivity and heart-rate variability in prediction of total cardiac mortality after myocardial infarction. Lancet 1998; **351**: 478–484
8) Lechat P, Hulot JS, Escolano S et al: Heart rate and cardiac rhythm relationships with bisoprolol benefit in chronic heart failure in CIBIS II trial. Circulation 2001; **103**: 1428–1433
9) Pfeffer MA, Pfeffer JM, Steinberg C et al: Survival after an experimental myocardial infarction: beneficial effects of long-term therapy with captopril. Circulation 1985; **72**: 406–412
10) Burkoff D, Sagawa K: Ventricular efficiency predicted by an analytic model. Am J Physiol 1986; **250**: R1021–R1027
11) Zhao G, Shen W, Xu X et al: Selective impairment of vagally mediated nitric oxide-dependent coronary vasodilation in conscious dogs after pacing-induced heart failure. Circulation 1995; **91**: 2655–2663
12) Kakinuma Y, Ando M, Kuwabara M et al: Acetylcholine from vagal stimulation protects cardiomyocytes against ischemia and hypoxia involving additive non-hypoxic induction of HIF-1α. FEBS Lett 2005; **579**: 2111–2118
13) Ando M, Katare RG, Kakinuma Y et al: Efferent vagal nerve stimulation protects heart against ischemia-induced arrhythmias by preserving connexin 43 protein. Circulation 2005; **112**: 164–170
14) Sato T, Kawada T, Inagaki M et al: New analytic framework for understanding sympathetic baroreflex control of arterial pressure. Am J Physiol 1999; **276**: H2251–H2261
15) Sato T, Kawada T, Shishido T et al: Novel therapeutic strategy against central baroreflex failure: a bionic baroreflex system. Circulation 1999; **100**: 299–304
16) Tanaka M, Nishikawa T: Arterial baroreflex function in humans anaesthetized with sevoflurane. Br J Anaesth 1999; **82**: 350–354
17) Keyl C, Schneider A, Hobbhahn J et al: Sinusoidal neck suction for evaluation of baroreflex sensitivity during desflurane and sevoflurane anesthesia. Anesth Analg 2002; **95**: 1629–1636
18) Tarkkila PJ, Kauknen S: Complications during spinal anesthesia: a prospective study. Reg Anesth 1991; **16**: 101–106